AD-A090 027 HUGHES AIRCRAFT CO TORRANCE CALIF F/G 9/5
HIGH EFFICIENCY DEFLECTION MODULATED MICROWAVE GENERATOR STUDY.(U)
JUL 80 T WESSEL-BERG, I TAMMARU F30602-79-C-0089
UNCLASSIFIED W-08322 RADC-TR-80-211 NL

1 OF 2
AD A 090027

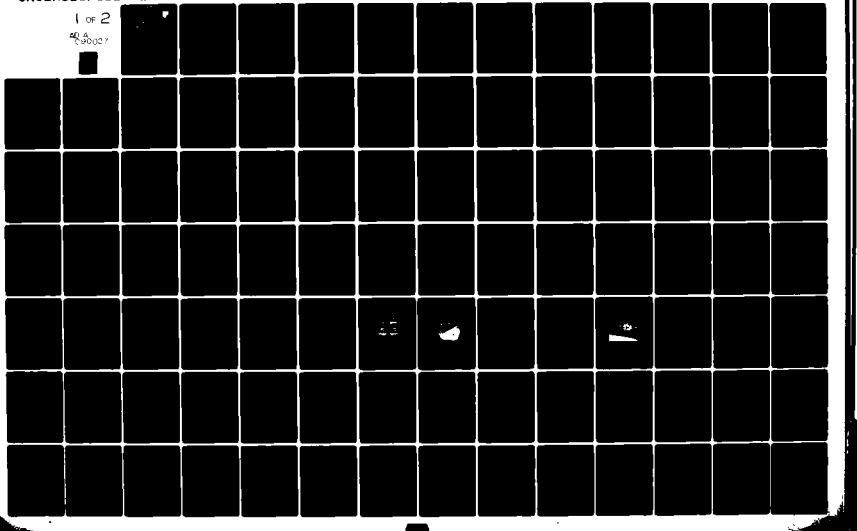

LEVEL II

RADC-TR-80-211
Final Technical Report
July 1980

HIGH EFFICIENCY DEFLECTION MODULATION MICROWAVE GENERATOR STUDY

Hughes Aircraft Company

T. Wessel-Berg
I. Tammaru

APPROVED FOR PUBLIC RELEASE; DISTRIBUTION UNLIMITED

Laboratory Directors' Fund No. LD9010C1

ROME AIR DEVELOPMENT CENTER
Air Force Systems Command
Griffiss Air Force Base, New York 13441

This report has been reviewed by the RADC Public Affairs Office (PA) and is releasable to the National Technical Information Service (NTIS). At NTIS it will be releasable to the general public, including foreign nations.

APPROVED: Kevin O'Brien

KEVIN O'BRIEN
Project Engineer

APPROVED: Frank J. Rehm

FRANK J. REHM
Technical Director
Surveillance Division

FOR THE COMMANDER: John P. Huss

JOHN P. HUSS
Acting Chief, Plans Office

SUBJECT TO EXPORT CONTROL LAWS

This document contains information for manufacturing or using munitions of war. Export of the information contained herein, or release to foreign nationals within the United States, without first obtaining an export license, is a violation of the International Traffic in Arms Regulations. Such violation is subject to a penalty of up to 2 years imprisonment and a fine of $100,000 under 22 U.S.C 2778.

Include this notice with any reproduced portion of this document.

If your address has changed or if you wish to be removed from the RADC mailing list, or if the addressee is no longer employed by your organization, please notify RADC (OCTP) Griffiss AFB NY 13441. This will assist us in maintaining a current mailing list.

Do not return this copy. Retain or destroy.

UNCLASSIFIED

SECURITY CLASSIFICATION OF THIS PAGE (When Data Entered)

(19) REPORT DOCUMENTATION PAGE		READ INSTRUCTIONS BEFORE COMPLETING FORM
1. REPORT NUMBER RADC-TR-80-211	2. GOVT ACCESSION NO. AD-A090	3. RECIPIENT'S CATALOG NUMBER 027
4. TITLE (and Subtitle) HIGH EFFICIENCY DEFLECTION MODULATED MICROWAVE GENERATOR STUDY		5. TYPE OF REPORT & PERIOD COVERED Final Technical Report February 79 — February 80
		6. PERFORMING ORG. REPORT NUMBER W-08322
7. AUTHOR(s) T. Wessel-Berg* I. Tammaru		8. CONTRACT OR GRANT NUMBER(s) F30602-79-C-0089
9. PERFORMING ORGANIZATION NAME AND ADDRESS Hughes Aircraft Company 3100 W. Lomita Blvd Torrance CA 90509		10. PROGRAM ELEMENT, PROJECT, TASK AREA & WORK UNIT NUMBERS 61101F LD9010C1
11. CONTROLLING OFFICE NAME AND ADDRESS Rome Air Development Center (OCTP) Griffiss AFB NY 13441		12. REPORT DATE July 1980 13. NUMBER OF PAGES 108
14. MONITORING AGENCY NAME & ADDRESS (if different from Controlling Office) Same		15. SECURITY CLASS. (of this report) UNCLASSIFIED 15a. DECLASSIFICATION DOWNGRADING SCHEDULE N/A

16. DISTRIBUTION STATEMENT (of this Report)

Approved for public release; distribution unlimited

17. DISTRIBUTION STATEMENT (of the abstract entered in Block 20, if different from Report)

Same

18. SUPPLEMENTARY NOTES

*Norwegian Institute of Technology, Trondheim, Norway
This effort was funded totally by the Laboratory Directors' Fund
RADC Project Engineer: Kevin O'Brien, 1Lt, USAF (OCTP)

19. KEY WORDS (Continue on reverse side if necessary and identify by block number)

Gyrocon	Deflection Modulated
Microwave Generator	Electric Deflection
High Gain	Multicavity Deflection
High Efficiency	
High Power	

20. ABSTRACT (Continue on reverse side if necessary and identify by block number)

This report describes a study of the deflection system in deflection modulated microwave generators (gyrocons).

A general deflection theory was developed, based on a relativistic beam formulation and a first order expansion of Maxwell's field equations. It includes the effect of dc space charge forces on the beam size as well as a distortion of the beam cross section due to the RF interaction. The

→ next page

DD FORM 1 JAN 73 1473 EDITION OF 1 NOV 65 IS OBSOLETE

UNCLASSIFIED

SECURITY CLASSIFICATION OF THIS PAGE (When Data Entered)

cont.

theory was applied to cavities with electric deflection fields. Such cavities were experimentally evaluated by cold tests and appear to be superior to the commonly used magnetic deflection cavities. A unique design approach makes it possible to achieve a circular beam deflection with a single RF signal. Multicavity deflection systems, in which the input cavity is followed by floating cavities that are excited by the deflection modulated beam, can provide high gain, typically 50-55 dB with three cavities.

General design curves relating optimum beam perveance to other operating parameters and desired conditions at the output ring resonator were derived, but the output cavity itself was not part of the study.

FOREWORD

The work reported herein was performed for Rome Air Development Center, Griffiss Air Force Base, New York, under Contract F30602-79-C-0089 with Lt. K. O'Brien (OCTP) as Project Engineer. Dr. T. Wessel-Berg, Professor of Physical Electronics at the Norwegian Institute of Technology, Trondheim, Norway, developed the theory and carried out the analysis of multicavity deflection systems. The experimental cold testing of deflection cavities was performed at the Electron Dynamics Division of Hughes Aircraft Company under the direction of Dr. I. Tammaru.

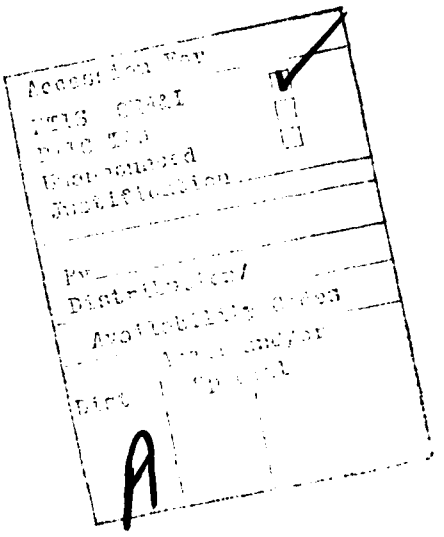

TABLE OF CONTENTS

TABLE OF CONTENTS (CONTINUED)

LIST OF ILLUSTRATIONS

LIST OF ILLUSTRATIONS (CONTINUED)

EVALUATION

This effort in support of TPO R4B resulted in significant progress in developing practical deflection modulated tubes (Gyrocons) for microwave radar applications. If utilized, these results could lead to high power microwave sources with extremely high efficiency.

Kevin O'Brien

KEVIN O'BRIEN
1Lt, USAF
Project Engineer

1.0 INTRODUCTION AND SUMMARY

This report is concerned with the deflection system in deflection modulated microwave generators. The name gyrocon has been coined for the original version of this kind of amplifier.[1,2,3,4] In a gyrocon, the electron beam is circularly deflected, causing it to describe an expanding helix, similar to a stream of water escaping through a nozzle which is rotated with a conical motion.

The chief attractive feature of gyrocons is high dc-to-RF conversion efficiency, with demonstrated values of greater than 80 percent. Because the electron beam is deflected rather than velocity modulated, almost all the kinetic beam power can be converted into RF power in an output ring resonator. The latter may be viewed as a waveguide bent around in a circle. The beam, which enters through a slit, is decelerated and almost completely slowed down by the electric field in the waveguide. By proper synchronization of the RF wave in the guide and the motion of the beam, a continuous energy conversion process takes place, while a directional coupler on the waveguide ring feeds out the RF power.

The present study encompassed the deflection system only. It did not include the output cavity, which presumably will be the subject of a follow-on program. But in anticipation of the use of a ring resonator, the analysis of the expanding beam was carried up to this point.

Two significant changes from the original gyrocon concept were explored. First, electric rather than magnetic deflection of the beam was considered. The deflection cavities are therefore of the open TE type instead of the TM type used in the original gyrocon. Cavities were cold tested during the program to verify the suitability of electric deflection. The second important feature was the use of a more general deflection system composed of several uncoupled deflection cavities in cascade. This leads to a considerable increase in gain, which becomes

comparable to that in klystrons. The additional gain in the floating cavities implies a larger deflection angle for the same input power. By these means it becomes feasible to eliminate the bulky dc magnetic deflection system used in the original gyrocon, and arrive at a substantially simpler and more attractive deflection amplifier.

The deflection theory described in this report is the transverse equivalent of the multicavity klystron amplifier, and the description in terms of beam and cavity parameters is quite analogous. Numerical data were obtained from a computer program that includes all important aspects of the deflection system and the subsequent drift space where the beam expands in a spiraling motion. The data are not limited to the basic deflection properties of the system, but also describe the expansion of the beam due to interior space charge and RF aberration caused by longitudinal stray fields in the cavities. The aberration manifests itself as a distortion of the circular beam cross section, and causes a focusing and defocusing of the expanding beam.

The results of the study indicate that deflection modulated RF amplifiers with high gain are feasible with a multicavity deflection system. Electric deflection appears to be superior to magnetic deflection. The devices are relatively simple physically, lacking dc magnetic focusing fields. They promise high conversion efficiency in general, and operate best at high power levels (hundreds of kilowatts and higher) and high voltages (a hundred kilovolts or more). The bandwidths are narrow. It should be possible to widen the frequency response by stagger tuning the deflection cavities, but this would need further study. Another possibility is to use coupled deflection cavities. For more definite performance predictions concerning efficiency and bandwidth, an analysis of the output cavity is needed. The output cavity is also likely to determine the practical high frequency limit of these devices, since the frequency constraints on the deflection system are not fundamentally different from those in other linear beam microwave tubes.

2.0 RELATIVISTIC THEORY OF BEAM DEFLECTION IN A GENERAL TRANSVERSE DEFLECTION SYSTEM

A very general deflection theory was developed during the program. In this section we shall summarize the main assumptions, equations and results.

A fairly thin relativistic beam passes through a transverse electromagnetic field, with no dc magnetic focusing field, and is subject to deflection. The variation of fields with distance along the axis is kept entirely arbitrary. This allows us to determine the overall deflection in a composite deflection system consisting of several separated cavities, i.e., a transverse klystron-type deflection system.

2.1 THE DYNAMIC EQUATIONS

The relativistically correct form of the momentum equation for an electron is

$$\frac{d}{dt}(m\vec{v}) = -e\,[\vec{E} + \vec{v} \times \vec{B}] \quad , \tag{2.1}$$

where the relativistic mass m is given by:

$$m = \frac{m_0}{\sqrt{1 - \frac{|\vec{v}|^2}{c^2}}} \tag{2.2}$$

Here, m_0 is the rest mass. For the deflection system it suffices to consider small signal conditions, which implies considerable simplification of (2.1) and (2.2). Let the total velocity be expressed in the form

$$\vec{v}(\vec{r}, t) = v_0\vec{a}_z + v_0\vec{U}(\vec{r}, t) \tag{2.3}$$

where v_0 is the dc velocity, in the z direction, and $\vec{U}(\vec{r}, t)$ is the normalized RF velocity.* The transverse components of $\vec{U}$ are best expressed in their circularly polarized form:

$$U_+ = U_x + jU_y \tag{2.4}$$

$$U_- = U_x - jU_y \tag{2.5}$$

It will also be convenient to normalize the axial distance z by the relation:**

$$Z = \beta_e z \ , \tag{2.6}$$

where $\beta_e = \omega/v_0$ is the usual electronic propagation factor, with $\omega = 2\pi f$.

We shall generally use normalized variables, partly because of the mathematical simplifications, but also because it more readily allows conclusions to be drawn concerning frequency scaling. The latter is an important question which has not yet been satisfactorily answered for this type of amplifier.

*With this definition the magnitude of the normalized RF velocity, U, is approximately equal to the deflection angle in radians.

**Our convention for all distance parameters will be lower case letters for physical coordinates, or lengths, and capital letters for the corresponding dimensionless parameters, using β_e^{-1} as the normalization constant throughout.

A first-order expansion of (2.1) and (2.2) yields the following set of momentum equations:

$$\frac{dU_+}{dZ} + jU_+ = -\frac{1}{V_0(1+\alpha)}\frac{1}{\beta_e}(E_+ + jv_0B_+) \tag{2.7}$$

$$\frac{dU_-}{dZ} + jU_- = -\frac{1}{V_0(1+\alpha)}\frac{1}{\beta_e}(E_- - jv_0B_-) \tag{2.8}$$

$$\frac{dU_z}{dZ} + jU_z = -\frac{\alpha^2}{V_0(1+\alpha)}\frac{1}{\beta_e}E_z \tag{2.9}$$

In these equations, α is the relativistic factor, defined by

$$\alpha = \sqrt{1 - \frac{v_0^2}{c^2}}\ , \tag{2.10}$$

and V_0 is the dc beam voltage. The polarized field components are defined in analogy with the velocities in (2.4) and (2.5).

Note that the extra relativistic factor α^2 in (2.9) reflects the fact that the longitudinal mass is larger than the transverse mass.

The equations of continuity, supplementing the momentum equations, are expressed in terms of the beam <u>displacement</u> $\vec{s}(\vec{r}, t)$, which is normalized as

$$\vec{S} = \beta_e\vec{s} \tag{2.11}$$

The basic equation of continuity is simply

$$\frac{\partial \vec{s}}{\partial t} + \vec{v}_0 \cdot \nabla \vec{s} = \vec{u} \quad , \tag{2.12}$$

which in normalized circularly polarized form becomes:

$$\frac{dS_+}{dZ} + jS_+ - U_+ = 0 \tag{2.13}$$

$$\frac{dS_-}{dZ} + jS_- - U_- = 0 \tag{2.14}$$

$$\frac{dS_z}{dZ} + jS_z - U_z = 0 \tag{2.15}$$

The overall set of dynamic equations consists of the momentum equations (2.7)-(2.9) and the equations of continuity (2.13)-(2.15).

2.2 EXPANSIONS OF THE ELECTROMAGNETIC FIELDS IN THE DEFLECTION SYSTEM

As pointed out it is imperative to maintain generality in the description of the electromagnetic fields. This will allow us to draw conclusions concerning the relative merits of electric and magnetic deflection systems. With a general field description the results are also readily applied to the special case of a multicavity deflection system.

The fields are expanded in their paraxial forms around the axis:

$$E_+(X, Y, Z) = \hat{E}_+^{(0)}(Z) + O(2) \tag{2.16}$$

$$B_+(X, Y, Z) = \hat{B}_+^{(0)}(Z) + O(2) \tag{2.17}$$

$$E_z(X, Y, Z) = \hat{E}^{(1)}_{zx} X + \hat{E}^{(1)}_{zy} Y + O(3) \tag{2.18}$$

$$B_z(X,Y,Z) = \hat{B}^{(1)}_{zx} X + \hat{B}^{(1)}_{zy} Y + O(3) \quad , \tag{2.19}$$

and similarly for the negative polarized components.

Using Maxwell's field equations in their general form, and applying the paraxial conditions (2.16)-(2.19), we obtain a set of differential equations, which have been solved for the transverse field components. More specifically, the driving term in the momentum equation (2.7) is obtained in the form

$$\hat{E}^{(0)}_{+}(Z) + jv_0 \hat{B}^{(0)}_{+}(Z)$$

$$= \int_{Z_1=0}^{Z} \hat{E}^{(1)}_{z+}(Z_1) \left[\cos \frac{v_0}{c} (Z - Z_1) + j \frac{v_0}{c} \sin \frac{v_0}{c} (Z - Z_1)\right] dZ_1$$

$$- \int_{Z_1=0}^{Z} c\hat{B}^{(1)}_{z}(Z_1) \left[\sin \frac{v_0}{c} (Z - Z_1) - j \frac{v_0}{c} \cos \frac{v_0}{c} (Z - Z_1)\right] dZ_1$$

(2.20)

A similar relation applies to the negative polarized driving term in (2.8), but henceforth we shall be concerned only with the positive polarized component.

The modes described by (2.20) can be considered as generalized TE and TM modes, actually a mixture of both. They are considerably more general than the usual TE and TM waveguide modes because there are no restrictions on the variations of the fields with respect to the axial distance Z. The equation specifies the transverse driving field $E_+ + jv_0B_+$ for any specified distribution of longitudinal electric and magnetic field gradients.

The virtue of (2.20) is primarily its generality, which permits us to draw general conclusions concerning the deflection taking place under certain specified conditions.

2.3 SOLUTION OF THE DYNAMIC EQUATIONS IN A GENERAL DEFLECTING FIELD

The general solution of the paraxial expansion of the dynamic equation (2.7) is:

$$\hat{U}_+^{(0)}(L) = -\frac{1}{V_0}\frac{1}{1+\alpha}\frac{1}{\beta_e}e^{-jL}\int_0^L e^{jZ}\left[\hat{E}_+^{(0)}(Z) + jv_0\hat{B}_+^{(0)}(Z)\right]dZ \tag{2.21}$$

The integral is taken from the input end Z = 0 of the deflection region, to the output end, specified by L. The fields are presumably zero at both end points of the deflection region.

An alternate formula for the velocity $\hat{U}_+^{(0)}$ can be obtained through substitution of the general relation (2.20) into (2.21). The result is simply

$$\hat{U}_+^{(0)}(L) = -\frac{1}{V_0}\frac{1}{1+\alpha}\frac{j}{\beta_e}e^{-jL}\int_0^L e^{jZ}\hat{E}_{z+}^{(1)}(Z)\,dZ \tag{2.22}$$

The two equations (2.21) and (2.22) represent alternative but equivalent expressions for the deflection of a beam in a general electromagnetic field. In particular, (2.22) is convenient for interpretation of the deflection in a generalized TE cavity, which is characterized by

$$\hat{E}_z^{(1)}(Z) = 0 \quad \text{everywhere} \tag{2.23}$$

In this case (2.22) reduces to

$$\hat{U}_+^{(0)}(L) = 0 \tag{2.24}$$

Hence, in a generalized TE-cavity the net deflection at the output end is zero. This is essentially Panofsky's result[5] which, however, should be interpreted cautiously. It is true only if (2.23) is strictly satisfied everywhere in the deflection space including the stray fields in the end regions. The often quoted belief that TE-type deflection systems cannot be used on account of (2.22)-(2.24), or reference 5, is not true. As an example, the parallel-plate deflecting cavities described later are nominally of the TE-type, with zero longitudinal electric field gradient $\hat{E}_{z+}^{(1)}$ in the deflecting region. However, the end-regions support stray fields having nonzero $E_z^{(1)}$ components, so that the condition (2.33) is not fulfilled. Therefore, deflection takes place, and $\hat{U}_+^{(0)}(L)$ is nonzero. Indeed, the TE parallel-plate cavity is a very efficient deflector, a fact which should be obvious from the low frequency version used in the analogous deflecting systems in cathode ray tubes.

On the basis of (2.21) serving as the fundamental equation, the other dynamic variables can be expressed in terms of $\hat{U}^{(0)}(L)$. The longitudinal velocity gradient $\hat{U}_{z+}^{(1)}(L)$ is given by

$$\hat{U}_{z+}^{(1)}(L) = -j\alpha^2\hat{U}_+^{(0)}(L) \tag{2.25}$$

The displacement components are obtained from the relations:

$$\hat{S}_{+}^{(0)}(L) = j\beta_e \frac{d}{d\beta_e} \hat{U}_{+}^{(0)}(L) \tag{2.26}$$

$$\hat{S}_{z+}^{(1)}(L) = \beta_e \alpha^2 \frac{d}{d\beta_e} \hat{U}_{+}^{(0)}(L) \tag{2.27}$$

These entirely general relations tell us the important result that the transverse velocity modulation $\hat{U}_{+}^{(0)}(L)$ is always accompanied by a longitudinal velocity gradient $\hat{U}_{z+}^{(1)}(L)$. At low dc voltage where $\alpha^2 = 1$, the magnitude of the velocity gradient is exactly equal to the transverse velocity modulation. As the voltage is increased towards the relativistic domain, the factor $\alpha^2 = 1 - v_0^2/c^2$ becomes successively smaller. Therefore, the unavoidable longitudinal velocity modulation is also smaller for relativistic velocities.

The physical reason why we are concerned with the longitudinal velocity gradient is that it gives rise to distortion of a finite size electron beam. The <u>longitudinal</u> velocity modulation of the electrons is proportional to their radial positions within the beam cross section. The resulting <u>bunching</u> and <u>overtaking</u> process in the drift space following the deflection region gives rise to various kinds of beam distortion or aberration phenomena, to be described later.

This concludes the discussion of the fundamental modulation taking place in any general transverse deflection system. In the next section the results are applied to a multicavity deflection system.

3.0 MULTICAVITY DEFLECTION SYSTEM

The basic analysis of the previous section is quite general, and is therefore applicable to the deflection system shown schematically in Figure 3.1. The configuration consists of a total of N cascaded, uncoupled cavities.

The input power P_i feeds the first cavity, setting up the RF voltage V_1 causing deflection of the beam. The deflected beam passes through the second, floating cavity and excites the RF voltage V_2, which causes further deflection of the beam. And so on through the N-1 floating cavities. The problem at hand is to determine the RF voltages in all the cavities, i.e., the voltage gains. Once these are determined, evaluation of the overall deflection is a straightforward matter using the general equations of Section 2.

3.1 CAVITY CONFIGURATIONS

A number of different cavity configurations were analyzed during the program. These were:

1. The double parallel plate cavity
2. The twisted parallel plate cavity
3. The vane resonator.

Configurations 1 and 3 were also cold tested. The vane resonator is a magnetron-type cavity that operates in a TE-type mode (not the usual magnetron mode). The mode is a true circularly polarized mode.

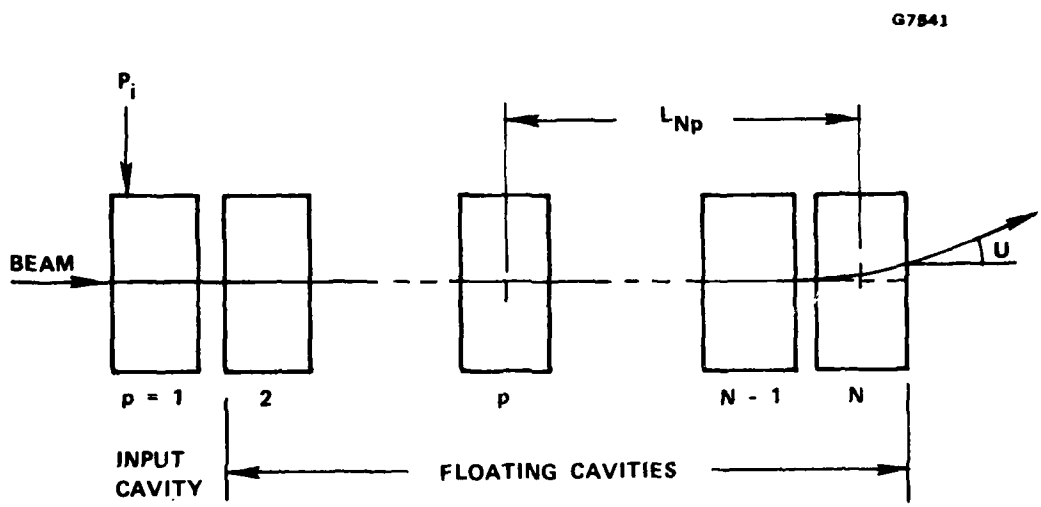

Figure 3.1 Sketch of the multicavity deflection system.

The cavities listed as 1 and 2 are variations of the same basic configuration. The double parallel plate cavity appears to combine geometric simplicity with good electrical characteristics. Furthermore, it does not need any special input couplers in order to excite a circularly polarized motion of the beam. The circular motion is obtained through an appropriate transit angle of $\pi/2$ between the two sets of plates.

For these reasons the double parallel plate cavity was chosen as the building block of the multicavity deflection system; the following analysis refers to this kind of cavity.

The basic elements of the cavity are shown in Figure 3.2. The second set of parallel plates is rotated 90 degrees with respect to the first set, while each plate of one set is in metallic contact with one plate of the other set. This ensures the same time phase of the electric fields in both plate sets. The circular motion of the beam is obtained by transit time effects rather than by truly circularly polarized fields.

The normalized plate length L_0 is less than or equal to $\pi/2$, and we put

$$L_0 = \xi \frac{\pi}{2} , \tag{3.1}$$

where ξ is less than or equal to unity.

Each cavity is characterized by a number of parameters. Let us define these in their general forms, which are applicable to any kind of deflection cavity.

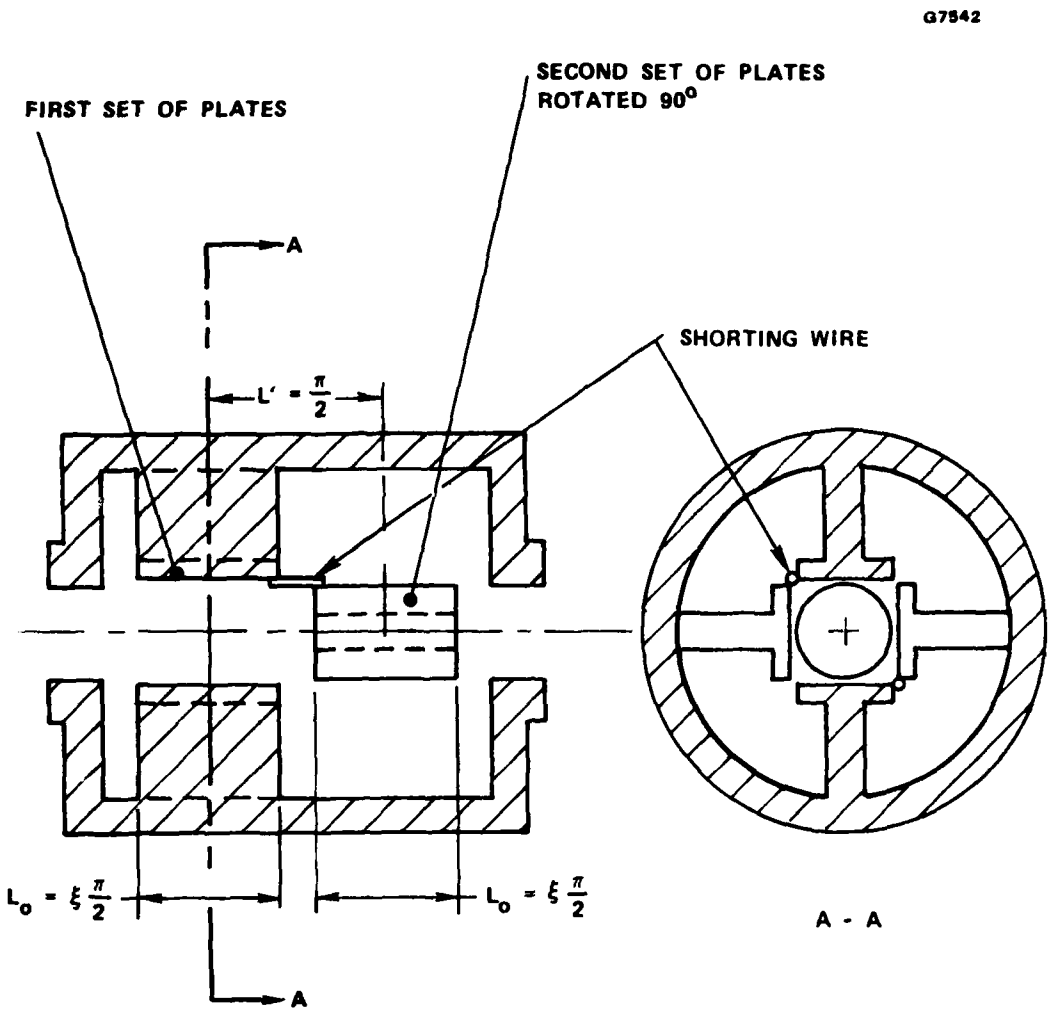

Figure 3.2 Basic geometry of the double parallel plate cavity.

3.2 CAVITY PARAMETERS

The RF voltage V_+ is defined by the general relation

$$V_+^2 = \ell \int_0^\ell \left| \hat{E}_+^{(0)}(z) + jv_0 \hat{B}_+^{(0)}(z) \right|^2 dz \,, \tag{3.2}$$

where ℓ is the total length of the cavity.

The coupling coefficient M_+ is specified by the Fourier transform of the field distribution:

$$M_+ = \frac{1}{V_+} \int_0^\ell \left[\hat{E}_+^{(0)}(z) + jv_0 \hat{B}_+^{(0)}(z) \right] e^{j\beta_e z} \, dz \tag{3.3}$$

The beam loading conductance G_{e+} is given by the expression

$$G_{e+} = -\frac{1}{4} \frac{I_0}{V_0} \frac{1}{1+\alpha} \beta_e \frac{d}{d\beta_e} [M_+ M_+^*] \tag{3.4}$$

The RF dissipation P in the cavity walls is

$$P = \frac{1}{2} G_c V_+^2 \,, \tag{3.5}$$

where G_c is the circuit conductance.

The Q-value of the cavity is

$$Q = \frac{\omega W}{P} \tag{3.6}$$

where W is the stored energy.

The characteristic impedance R_{sh}/Q is obtained from (3.5) and (3.6):

$$\frac{R_{sh}}{Q} = \frac{1}{2\omega}\frac{V_+^2}{W} \tag{3.7}$$

The circuit admittance is defined by

$$Y_c = \left(\frac{Q}{R_{sh}}\right)\frac{1}{Q_L} + 2j\left(\frac{Q}{R_{sh}}\right)\frac{\omega - \omega_0}{\omega_0} \quad , \tag{3.8}$$

where ω_0 is the resonant frequency and Q_L is the loaded Q of the cavity.

In addition to the listed parameters, which apply to each individual cavity, we also need the transfer admittance Y_{np} between cavity n and cavity p, where $n \leq N$ and $p < n$:

$$Y_{np} = -\frac{1}{2}\frac{I_0}{V_0}\frac{1}{1+\alpha}\beta_e\frac{d}{d\beta_e}\left[M_{+n}^* M_{+p}^* e^{-j\beta_e \ell_{np}}\right] \tag{3.9}$$

The parameters listed here in a cursory manner, in particular those relating to the beam, evolve in a natural way from a consistent but somewhat lengthy analytical treatment of the interactions taking place in the multicavity deflection section.

3.3 THE VOLTAGE GAIN IN THE MULTICAVITY DEFLECTION SYSTEM

The voltage gain is obtained by matching the beam power and the circuit power in each of the N cavities constituting the system. This procedure gives us a set of N equations to determine the RF voltages in the cavities.

Defining the voltage gain η_p of the p^{th} cavity by

$$\eta_p = \frac{V_{+p}}{V_{+1}} , \tag{3.10}$$

we find that η_p is given by the following determinant:

$$\eta_p = \begin{vmatrix} \eta_{21}, & -1, & 0, & 0 & \cdots & 0 \\ \eta_{31}, & \eta_{32}, & -1, & 0 & \cdots & 0 \\ \vdots & & & & & \vdots \\ \eta_{p-2,1}, & \eta_{p-2,2} & \cdots & -1, & & 0 \\ \eta_{p-1,1}, & \eta_{p-1,2} & \cdots & \eta_{p-1,p-2}, & & -1 \\ \eta_{p,1}, & \eta_{p,2} & \cdots & \eta_{p,p-2}, & & \eta_{p,p-1} \end{vmatrix}$$

$$p = 2, 3 \ldots N \tag{3.11}$$

The elements in the determinant are specified by

$$\eta_{s,r} = - \frac{y_{sr}}{g_{e+s} + y_{cs}} \tag{3.12}$$

where y_{sr}, g_{e+s}, and y_{cs} are the normalized versions of Y_{sr}, G_{e+s}, and $Y_{c,s}$, the normalization being with respect to the dc beam conductance $G_0 = I_0/V_o$.

Since the voltage gain is referred to the RF voltage V_{+1} in the input cavity, it is necessary to relate V_{+1} to the input power P_i driving the cavity. The following relation applies:

$$\left(\frac{V_{+1}}{V_0}\right)^2 = 2\,\frac{P_i}{P_0}\,\frac{1}{g_{e+s} + g_{c1}} \quad , \tag{3.13}$$

where we have assumed that the cavity is tuned to resonance.

3.4 THE DEFLECTION SENSITIVITY OF THE MULTICAVITY SYSTEM

Having determined the RF voltages of the set of floating cavities from (3.11) it is a fairly simple matter to evaluate the transverse velocity $\hat{U}_+^{(0)}$ and the corresponding displacement $\hat{S}_+^{(0)}$ at the exit end.

Let us define the deflection sensitivity $\delta\hat{U}_{+n}^{(0)}$ by

$$\delta\hat{U}_{+n}^{(0)} = \frac{\hat{U}_{+n}^{(0)}}{\left(\frac{V_{+1}}{V_0}\right)} \quad , \tag{3.14}$$

and the displacement sensitivity $\delta\hat{S}_{+n}^{(0)}$ by

$$\delta\hat{S}_{+n}^{(0)} = \frac{\hat{S}_{+n}^{(0)}}{\left(\frac{V_{+1}}{V_0}\right)} \tag{3.15}$$

These variables represent the normalized transverse deflection variables for a relative input voltage V_{+1}/V_0 of unity, i.e., for an RF voltage V_{+1} equal to the dc voltage V_0.

Using the previously established general deflection theory in conjunction with the gain expressions, we obtain the following deflection and displacement sensitivities at the exit of the last cavity:

$$\delta\hat{U}_{+N}^{(0)} = -\frac{1}{1+\alpha}\sum_{p=1}^{N} e^{-j(L_{Np}+L_N/2)} M_{+p}\,\eta_p \quad , \tag{3.16}$$

where L_N is the length of the Nth cavity.

$$\delta\hat{S}_{+N}^{(0)} = -\frac{1}{1+\alpha}\sum_{p=1}^{N} e^{-j(L_{Np}+L_N/2)}\left[(L_{Np}+L_N/2)\,M_{+p} + j\beta_e \frac{dM_{+p}}{d\beta_e}\right]\eta_p \tag{3.17}$$

These expressions simply sum up the contributions from all the N cavities constituting the deflection system.

Analytical evaluation of the deflection sensitivity and the displacement sensitivity from (3.16) and (3.17) is prohibitive, and a computer program was written to undertake this task. The program supplies considerably more data than $\delta\hat{U}_{+N}$ and $\delta\hat{S}_{+N}$ alone; it is described in greater detail in later sections.

In conclusion of this section, let us summarize the achievements. We have developed a general theory of deflection in a composite deflection system consisting of any number N of uncoupled, cascaded cavities. Each cavity is specified by its circuit parameters which are the characteristic impedance R_{sh}/Q, its unloaded Q-value, and its detuning parameter $\delta = (\omega - \omega_\theta)/\omega_0$. The theory predicts the deflection and displacement at the exit end for a given input power P_i.

The theory is the transverse equivalent of the usual multicavity klystron theory. Although the formal theories for the two are quite similar, there are important differences arising from the different nature of the beam modes.

In the usual klystron the beam supports one fast and one slow space charge mode. In the transverse system the two modes involved are degenerate in the sense that both propagate with the dc beam velocity. The first mode is a pure displacement mode with zero transverse velocity. Hence, this mode does not grow with distance in the subsequent drift space and for this reason is of minor importance. The excitation of this pure displacement mode is described by the last term in the bracketed expression in (3.17).

The second transverse mode is described by a constant transverse velocity and a linearly growing displacement proportional to the velocity. Its excitation is described by (3.16) as far as the velocity is concerned, and by the first term in (3.17), which is the linearly growing displacement. This mode is the one that describes the expanding spiraling motion in the drift space of the deflection amplifier.

The degeneracy of the two modes and the accompanying linear growth with distance causes an essential difference in the details of the transfer characteristics compared to the ordinary klystron. In the klystron, the interference between the two space charge modes causes several undesirable beating effects such as zero's in the complex transfer characteristics, and a fairly sensitive and critical dependence of transfer characteristics on cavity spacings.[6]

These effects are entirely absent in the deflection amplifier, where the transverse modulation always grows with distance. Therefore, no cancellation effects take place, and the zeros in the transfer characteristics

are absent. There is no optimum spacing between cavities; the gain simply increases linearly with the spacing.

The absence of undesirable zeros in the complex transfer characteristics is a very attractive feature of the deflection modulated amplifier. It implies flexibility in geometric design, and simpler broadbanding procedures. Even if we deal exclusively with multicavity deflection systems in the present report, it is perhaps appropriate to point out that simplifications of the same nature would occur in traveling-wave deflection systems. Such systems have not yet been proposed or analyzed, but could conceivably be of interest as high-efficiency broadband amplifiers.

4.0 THE BEAM DYNAMICS IN THE DRIFT SPACE

The configuration of the last cavity and the subsequent drift space are shown schematically in Figure 4.1. Also shown is the longitudinal coordinate Z with Z = 0 at the exit end of the last cavity.

The input conditions for the spiraling motion in the drift space are the normalized velocity $\hat{U}^{(0)}_{+N}$ (the absolute value of which is equal to twice the deflection angle in radians) and displacement $\hat{S}^{(0)}_{+N}$. The values of the same variables at the location Z are given by

$$\hat{U}^{(0)}_{+}(Z) = \hat{U}^{(0)}_{+N}\, e^{-jZ} \tag{4.1}$$

$$\hat{S}^{(0)}_{+}(Z) = \left[\hat{S}^{(0)}_{+N} + Z\hat{U}^{(0)}_{+N}\right] e^{-jZ} \tag{4.2}$$

These equations describe the trajectories of the center electrons in the finite-size beam, as indicated in Figure 4.1. These are not subject to any longitudinal forces in the deflection system and are, therefore, moving with the longitudinal dc velocity v_0. The off-axis electrons are exposed to longitudinal stray fields and are, therefore, velocity modulated. The subsequent drift and bunching give rise to beam distortion phenomena. These are important in determining beam size and shape at the end of the drift region where the output cavity is located.

The longitudinal modulations are specified by the general formulae (2.25) and (2.27). In the drift space they are given by

$$\hat{U}^{(1)}_{z+}(Z) = -j\alpha^2\hat{U}^{(0)}_{+}(Z) \tag{4.3}$$

$$\hat{S}^{(1)}_{z+}(Z) = -j\alpha^2\hat{S}^{(0)}_{+}(Z) \tag{4.4}$$

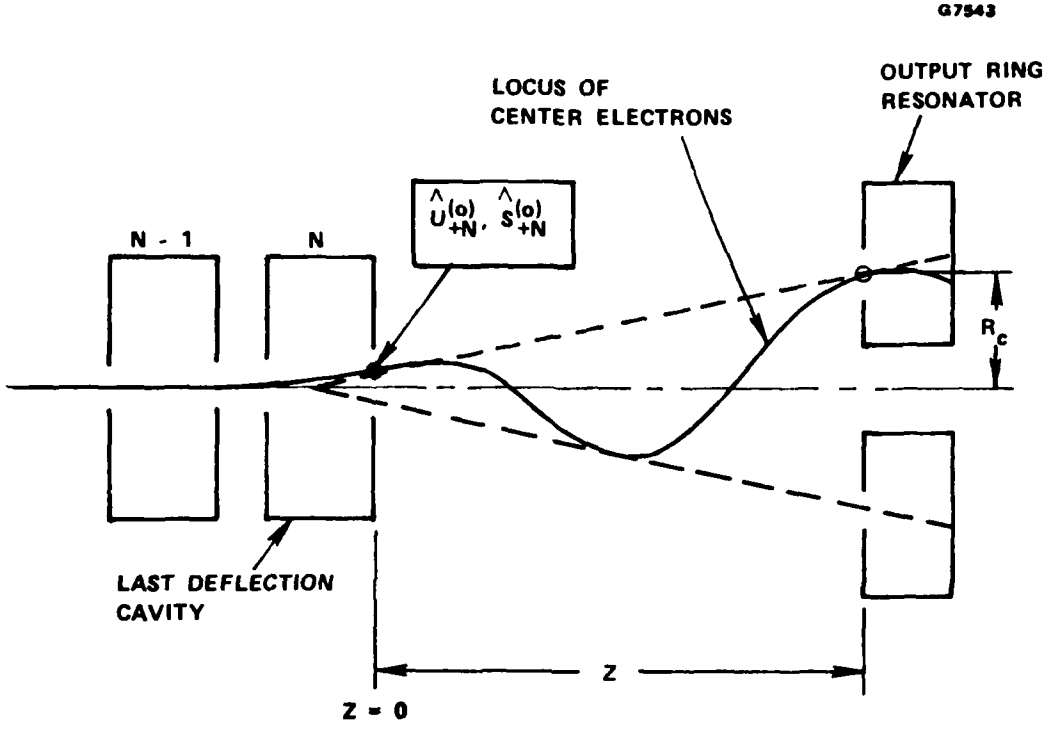

Figure 4.1 Schematic illustration of the last deflection cavity, the drift space, and the output cavity. Also shown is the locus of the center electrons at an instant in time. (The actual trajectory of a center electron in the drift space is a straight line.)

These equations relate the longitudinal velocity and displacement gradients to the actual transverse modulations. Note that the equations (4.1)-(4.4) specify complex amplitudes of the relevant paraxial expansions of the actual RF variables.

4.1 THE RF DYNAMIC VARIABLES IN THE DRIFT SPACE

The actual real variables as a function of the normalized undisplaced coordinates X, Y, Z and time T = ωt are obtained from (4.1)-(4.3). Let us write the two complex input variables $\hat{U}^{(0)}_{+N}$ and $\hat{S}^{(0)}_{+N}$ as follows:

$$\hat{U}^{(0)}_{+N} = U_N e^{j\theta} \tag{4.5}$$

$$\hat{S}^{(0)}_{+N} = S_N e^{j\phi} \tag{4.6}$$

Here U_N and S_N are the absolute values, and θ and ϕ the phase angles. In terms of those variables we obtain the following transverse components:

$$U_x(Z, T) = \frac{1}{2} U_N \cos (T - Z + \theta) \tag{4.7}$$

$$U_y(Z, T) = \frac{1}{2} U_N \sin (T - Z + \theta) \tag{4.8}$$

$$S_x(Z, T) = \frac{1}{2} S_N \cos (T - Z + \phi) + \frac{1}{2} U_N Z \cos (T - Z + \theta) \tag{4.9}$$

$$S_y(Z, T) = \frac{1}{2} S_N \sin (T - Z + \phi) + \frac{1}{2} U_N Z \sin (T - Z + \theta) \tag{4.10}$$

The longitudinal components are obtained from (4.3) and (4.4):

$$U_z(X, Y, Z, T) = \frac{1}{2}\alpha^2 U_N [X \sin(T - Z + \theta) - Y \cos(T - Z + \theta)] \tag{4.11}$$

$$S_z(X, Y, Z, T) = -\frac{1}{2}\alpha^2 S_N [Y \cos(T - Z + \phi) - X \sin(T - Z + \phi)] - \frac{1}{2}\alpha^2 U_N Z [Y \cos(T - Z + \theta) - X \sin(T - Z + \theta)] \tag{4.12}$$

These relations are quite general and show that all the velocity and displacement components, including the longitudinal ones, are expressed in terms of the corresponding transverse components at the exit of the deflection region, namely U_N and S_N and their phases θ and ϕ. The equations describe all the details of the dynamics of the outwardly spiraling beam, including distortion of the beam cross section caused by the longitudinal modulation. This particular phenomenon is important for the determination of the beam size and shape at the location of the output cavity, a subject which is disucssed in the next section.

4.2 BEAM DISTORTION AND RF FOCUSING

A particular electron in the beam is specified by its undisplaced coordinates X, Y, and Z at time T. These are the coordinates entering in (4.1)-(4.12) because we have consistently used the displacement, or polarization, description of the beam dynamics.

When the beam is deflected due to RF modulation, the same electron finds itself at the vectorial position $\vec{R}_D$ specified by the general r lation:

$$\vec{R}_D = \vec{R} + \vec{S}\ (\vec{R},\ T) \tag{4.13}$$

The components of this equation are:

$$X_D(X,\ Z,\ T) = X + S_x(Z,\ T) \tag{4.14}$$

$$Y_D(Y,\ Z,\ T) = Y + S_y(Z,\ T) \tag{4.15}$$

$$Z_D(X,Y,Z,T) = Z + S_z(X,\ Y,\ Z,\ T) \tag{4.16}$$

In these expressions it is important to emphasize that X, Y, Z are the undisplaced coordinates, and that X_D, Y_D and Z_D are the displaced *coordinates. We* are interested in the shape of the beam cross section at a given position along the axis which is specified by the coordinate Z_D and not Z. This implies that one has to determine the particular undisplaced positions Z which give rise to the displaced position Z_D. The relation between the two is given by (4.16). By invoking (4.12) as well, the following relation is obtained:

$$Z - \frac{1}{2}\,\alpha^2 S_N\,[Y\cos(T - Z + \phi) - X\sin(T - Z + \phi)]$$

$$-\frac{1}{2}\,\alpha^2 U_N Z\,[Y\cos(T - Z + \phi) - X\sin(T - Z + \phi)] = Z_D \tag{4.17}$$

This is a transcendental equation in Z which has to be solved for Z as a function of the presumably constant values of Z_D, X, Y, and T. The iteration procedure required in solving the transcendental equation is part of the computer program.

Let us formally express the result as the mathematical function:

$$Z = Z_D + \Delta(X, Y, Z_D, T) \quad , \tag{4.18}$$

where $\Delta(X, Y, Z_D, T)$ is nonzero for a finite size beam, i.e., for X and Y different from zero.

The actual beam cross section at the fixed position Z_D is obtained by inserting (4.18) to (4.14) and (4.15), and using the relations (4.9) and (4.10). In so doing, it is clear that the amount of distortion of the original circular beam cross section is described by the magnitude of the function $\Delta(X, Y, Z_D, T)$. The details of the functional variations are rather involved, but a number of general features are readily apparent. On the basis of these the following trends can be stated:

1. The distortion increases with X and Y and hence with the original beam size.

2. The distortion increases with the deflection angle U_N and with the displacement S_N at the exit of the deflection region.

3. The distortion increases with distance Z_D in the drift space.

4. The distortion is smaller at relativistic velocities, because of the factor α^2 in (4.17).

5. At any location Z_D in the drift space we can always identify one particular diameter in the beam along which the electrons retain the same relative positions as in the original circular beam.

The last statement is proved as follows.

Let us specify the electron positions along a particular diameter in the original beam by the relations

$$X = R_p \cos \gamma$$

$$Y = R_p \sin \gamma \qquad (4.19)$$

where γ is some constant angle, and R_p is the position of the p^{th} electron from the beam center.

Proceeding to put $\Delta(X, Y, Z_D, T)$ equal to zero, and therefore also $Z = Z_D$, we obtain the equation

$$S_N \sin (\gamma - T + Z_D - \phi) + U_N Z_D \sin (\gamma - T + Z_D - \theta) = 0 \qquad (4.20)$$

This equation always has a solution for γ depending on the particular choice of Z_D and T, but is independent of R_p. Hence, the statement in 5 is proved.

One important consequence of this result is the occurrence of a focusing and defocusing of the beam as it traverses the drift space.

The described effects are demonstrated in Figure 4.2 showing the cross section of the spiraling beam as it progresses down the drift space. The figure refers to the following input conditions:

$$U_N = 0.2, \text{ i.e., } U = 0.1$$

$$S_N = 0$$

$$\phi = \theta = 0 \ , \qquad (4.21)$$

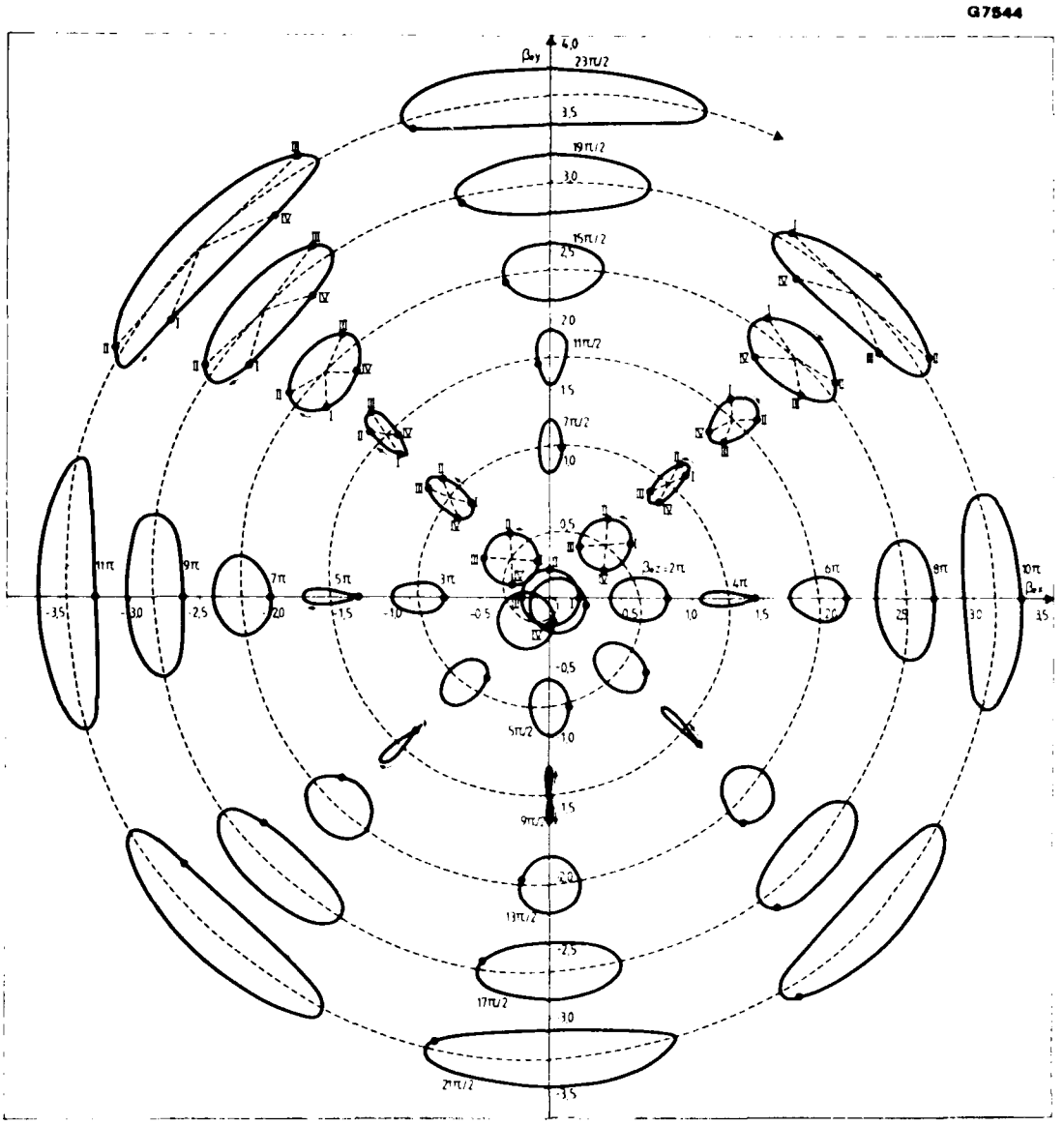

Figure 4.2 Figure illustrating the RF distortion taking place in the deflected beam due to longitudinal modulation. Deflection angle U = 0.1 radians, normalized beam radius R_0 = 0.2.

and a normalized beam radius $R_0 = 0.2$. The cross sections shown in the figure are labeled with the normalized longitudinal position Z_D, and the X and Y axes are the transverse positions.

The effect described in statement 5 above is readily apparent. The beam mantains its size in the radial direction, but exhibits a focusing and defocusing in the angular direction. Beyond a certain point the angular size gets progressively larger as the beam traverses the drift space.

The RF focusing effect can be used to advantage in obtaining a small beam size at the location of the output cavity. Typically, the required normalized radius of the circular traveling-wave cavity is $R_c=2$. It follows from Figure 4.2 that the beam happens to be focused for $R_c \leq 2$. This situation is quite fortunate in that a small beam size is an important factor in obtaining high efficiency in the energy conversion taking place in the output cavity.

We shall later present graphs of the distorted beam cross section for several proposed multicavity deflection systems. These also include the additional effect of space charge defocusing effects to be described next.

4.3 BEAM EXPANSION DUE TO SPACE CHARGE

Up to this point space charge forces have been disregarded. The main effect of these is to cause a circularly symmetric beam expansion due to the dc space charge. The RF space charge forces are disregarded because they are much smaller than the dc forces.

Using relativistically correct dynamic equations, the following universal beam spread equation is obtained:

$$f\left(\frac{r}{r_0}\right) = C_1 \left(\frac{I_0}{V_0^{3/2}}\right)^{1/2} \left(\frac{2\alpha}{1+\alpha}\right)^{3/4} \left(\frac{z}{r_0}\right) , \qquad (4.22)$$

with

$$f\left(\frac{r}{r_0}\right) = \int_0^{\sqrt{\ln(r/r_0)}} e^{w^2}\, dw \qquad (4.23)$$

Here r_0 is the minimum beam radius, z is the distance measured from the beam minimum, $I_0/V_0^{3/2}$ is the beam perveance, and the factor involving α represents a relativistic correction. The factor is unity at low voltage where $\alpha = 1$, and approaches zero for extreme relativistic speeds, where α is zero. Hence, as expected, the beam expansion is less serious in the relativistic domain. The constant C_1 is given by

$$C_1 = \left(8\pi\varepsilon_0 \sqrt{2e/m_0}\right)^{-1/2} \qquad (4.24)$$

$$= 87.04 \text{ in SI units.}$$

For small beam expansions,

$$f\left(\frac{r}{r_0}\right) \approx \sqrt{\frac{r}{r_0} - 1} \qquad (4.25)$$

so that

$$\frac{R}{R_0} \approx 1 + C_1^2 \left(\frac{I_0}{V_0^{3/2}}\right)\left(\frac{2\alpha}{1+\alpha}\right)^{3/2}\left(\frac{Z}{R_0}\right)^2 \qquad (4.26)$$

In this expression the radii and the axial distance have been converted to normalized form.

The universal beam spread curve and the approximate expression (4.26) have been plotted in Figure 4.3. Note that the factor $(I_0/V_0^{3/2})_{\mu P}$ is the microperveance. For a typical beam expansion of a factor of two, the approximate expression overestimates the beam size by 7 percent. This is quite acceptable for our present purpose, and it will be convenient to use (4.26) in subsequent analysis.

If we look at the trajectory of an edge electron through the deflection cavities, it approximately follows the parabolic beam spread curve in Figure 4.3. Therefore, the electron is subject to electromagnetic deflection fields which are slightly different from the ones corresponding to the assumed trajectory parallel with the axis. However, for moderate beam expansions, the effect on the transverse deflection taking place in the cavities is entirely negligible. The reason for the insensitivity to variations in the radial position is the nature of the transverse deflection fields. To the lowest order, used in the present deflection theory, the fields are constant and independent of the radial position.

On the other hand, the longitudinal forces are proportional to the radial position. Therefore, the space charge beam expansion has some effects on the longitudinal modulation accompanying the basic transverse modulation.

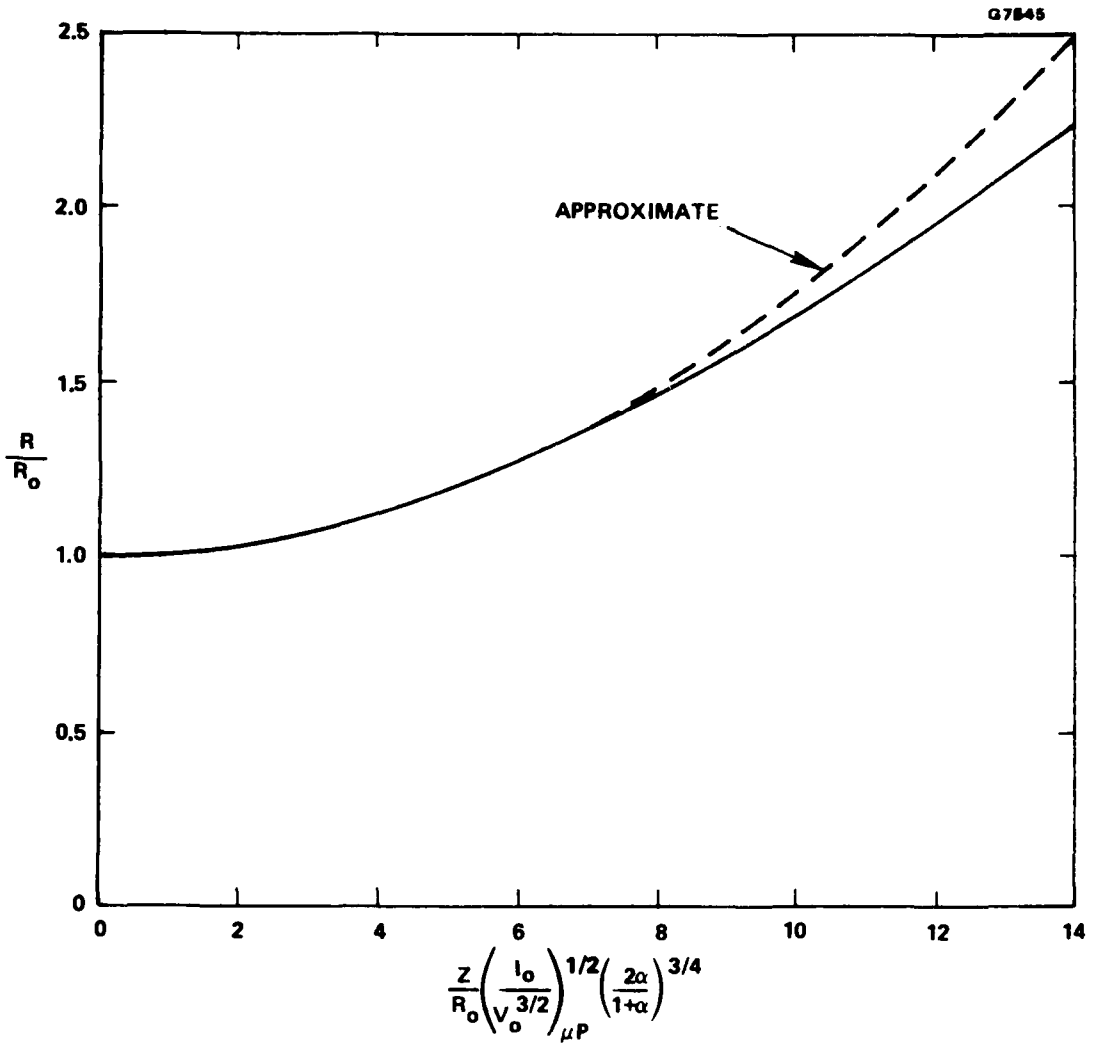

Figure 4.3 Relativistically correct universal beam spread curve, with the relative beam radius R/R_0 plotted vs the expression on the horizontal axis. The factor $(I_0/V_0^{3/2})_{\mu P}$ is the microperveance.

The following conclusions are drawn from this discussion. The space charge beam expansion has practically no effect on the beam deflection and, therefore, the gain is not affected. The longitudinal modulation is affected to some extent, and this is expected to cause some minor modifications in the rf beam focusing effect described in Section 4.2. But the focusing effect is not a major factor in the overall properties of the deflection system. Hence, we may conclude that the major effect of the space charge beam expansion is to cause an enlarged beam cross section at the position of the output cavity. The enlargement should be kept as small as possible, in order to retain a narrow beam and high efficiency of the energy conversion process in the output cavity.

In the computer program the space charge beam expansion is simply superimposed on the RF focused beam. In view of the discussion above this procedure is sufficiently accurate for characterizing the deflection system.

From inspection of Figure 4.3, it is clear that the relevant parameters in determining beam spread are the perveance and the ratio Z/R_0. The relativistic factor $(2\alpha/1 + \alpha)^{3/4}$ does not differ much from unity except for extremely high voltages (at V_0 = 90 kV the factor is equal to 0.94) and is, therefore, not of essential importance. In the next section, dealing with design considerations, we shall use the universal beam spread curve to establish some simple design criteria for the various parameters.

5.0 DESIGN CONSIDERATIONS AND PERFORMANCE LIMITS

The main design goals for the deflection system and the subsequent drift space are the following:

1. To develop a multicavity deflection system with gain comparable to ordinary klystrons, i.e., of the order of 40-60 dB.

2. To provide a rotating beam at the exit of the drift space with a normalized excursion radius R_c of approximately two; and with reasonably small normalized beam radius R at this location.

The condition on the excursion radius R_c relates to the requirement that the circumference of the output ring resonator be equal to one wavelength. This is expressed by

$$2\pi r_c = \frac{v_{ph}}{f} , \tag{5.1}$$

where v_{ph} is the circumferential phase velocity in the ring waveguide. The normalized ring radius is then

$$R_c = \beta_e r_c = \frac{v_{ph}}{v_0} \tag{5.2}$$

Since the phase velocity in the guide is greater than c and the electron velocity is less than c, the normalized ring radius is generally greater than unity. In a low voltage device, operating at 100 kV for example, a value of approximately two might be typical.

Additional objectives in the design study are:

3. To establish the maximum beam perveance that can be used.
4. To determine the maximum frequency of operation.

We begin by considering the beam perveance and related parameters.

5.1 LIMITATIONS ON THE BEAM PERVEANCE

We shall make the reasonable assumption that the beam minimum is located at the exit of the deflection cavities. This assumption is justified by the fact that the transverse beam displacement becomes successively larger as the beam traverses the deflection cavities. Placing the beam minimum at the exit is an insurance against beam interception by the deflection plates of the last cavity.

With this assumption, i.e., with the beam minimum at $Z = 0$ in Figure 4.1, we can use the universal beam spread curve to determine the dc beam size R at the position Z of the output cavity. Or conversely, by a specified beam size R at the output cavity we can determine the minimum beam radius R_0 at $Z = 0$. This latter procedure is of much greater interest for design purposes. Using the approximate expression (4.26) we obtain a second order equation in terms of the ratio R_0/R. The solution is

$$\frac{R_0}{R} = \frac{1}{2} \pm \left[\frac{1}{4} - C_1^2 \left(\frac{Z}{R} \right)^2 \frac{I_0}{V_0^{3/2}} \left(\frac{2\alpha}{1+\alpha} \right)^{3/2} \right]^{1/2} \qquad (5.3)$$

The equation takes a particularly convenient form by introducing the deflection angle U and the excursion radius R_c at the location of the

output cavity. Since U is always small, the following equation applies:

$$Z = \frac{R_c}{U} \tag{5.4}$$

By means of this relation, (5.3) can be expressed in the desired form:

$$\frac{R_0}{R} = \frac{1}{2} \pm \left[\frac{1}{4} - 0.0303 \frac{1}{\left(\frac{2R}{R_c}\right)^2} \frac{1}{U^2} \left(\frac{I_0}{V_0^{3/2}} \right)_{\mu P} \left(\frac{2\alpha}{1+\alpha} \right)^{3/2} \right]^{1/2} \tag{5.5}$$

The ratio $2R/R_c$ appearing under the square root sign has the physical significance of "bunch width", measured in radians. As shown in Figure 5.1 the bunch width is the azimuthal length of the beam measured along the circumference of the output resonator. (RF focusing effects are disregarded in the present discussion.) A bunch length of unity corresponds to about 60 degrees. This is considerably better than the best bunches in a klystron which typically are twice this value. The bunch length has a bearing on the expected efficiency and, accordingly, is an important design parameter. For the present system it should be of the order of unity or less.

It is useful to obtain a graph of the expression (5.5) in the form of a universal curve. In Figure 5.2 the ratio R_0/R is plotted vs. the product appearing under the square root in (5.5). The product contains the following design parameters:

i) The <u>bunch length</u> $2R/R_c$ at the output cavity measured in radians

ii) The <u>deflection angle U</u>.

G7846

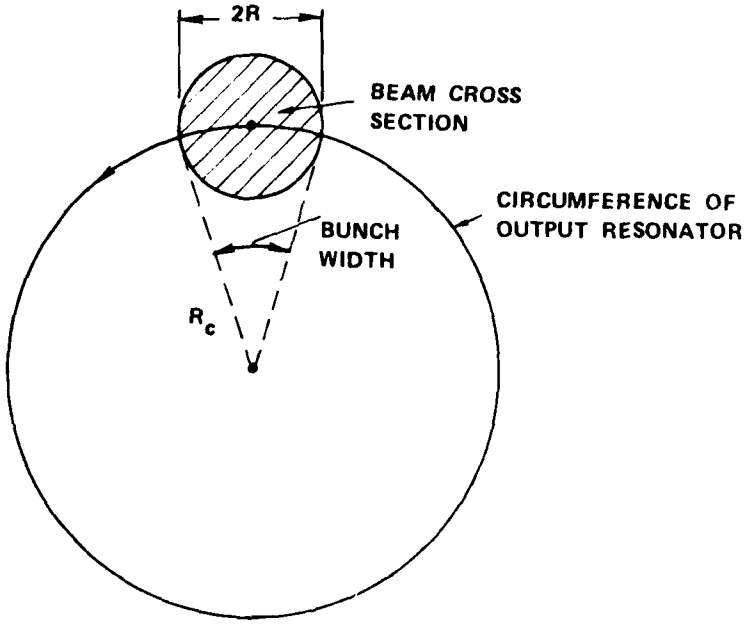

Figure 5.1 Illustration of the concept of "bunch width" of the rotating beam.

iii) The <u>beam perveance</u> $(I_0/V_0^{3/2})_{\mu P}$, expressed in microperveance.

iv) The <u>relativistic factor</u> $(2\alpha/1 + \alpha)^{3/2}$.

It is a reasonable choice to take the product plotted along the horizontal axis in Figure 5.2 as a <u>figure of merit M</u>:

$$M = \frac{1}{(2R/R_c)^2} \frac{1}{U^2} \left(\frac{I_0}{V_0^{3/2}}\right)_{\mu P} \left(\frac{2\alpha}{1 + \alpha}\right)^{3/2} \tag{5.6}$$

Apparently, the design should aim at maximizing M because this condition gives: i) the smallest bunch width for a given perveance or, ii) the highest perveance for a given bunch width, or iii) the smallest required deflection angle, and thereby the highest gain, for specified perveances and bunch widths.

Now, with this in mind it follows from Figure 5.2 that the figure of merit cannot exceed 8.25, which therefore represents the optimum design condition.

$$M_{max} = 8.25 \tag{5.7}$$

Let us express this condition explicitly by the design parameters:

$$\left(\frac{I_0}{V_0^{3/2}}\right)_{\mu P\ max} = 8.25\ U^2 \left(\frac{2R}{R_c}\right)^2 \left(\frac{1 + \alpha}{2\alpha}\right)^{3/2} \tag{5.8}$$

This is the maximum perveance for given values of the other parameters. The formula is quite significant for determining the performance limits.

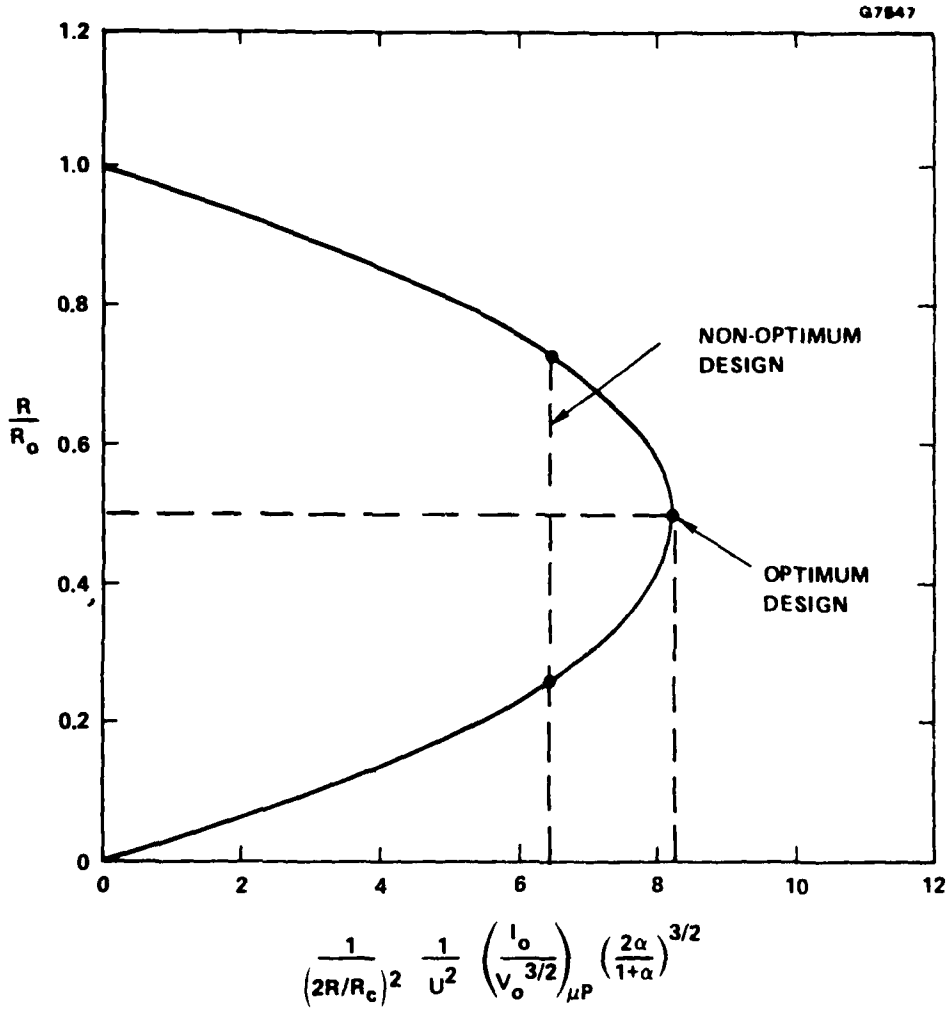

Figure 5.2 Universal curve specifying the minimum beam radius for a given set of design parameters.

If the amplifier is designed with $M < M_{max}$ it follows from Figure 5.2 that there are two possible values of the ratio R_0/R giving the same beam size R at the output cavity. These are located symmetrically around the optimum value of $R_0/R = 0.5$, with $M = M_{max} = 8.25$. Hence, for the optimum design

$$\left(\frac{R_0}{R}\right)_{opt} = 0.5 \quad , \tag{5.9}$$

which corresponds to a relative beam expansion of two in the drift space. In terms of the output resonator radius R_c and the bunch width $2R/R_c$, the optimum beam minimum is

$$(R_0)_{opt} = 0.25\ R_c\left(\frac{2R}{R_c}\right) \tag{5.10}$$

In Figure 5.3 we have plotted the expression in (5.8) as universal design curves for optimum performance. The beam perveance and dc beam power are normalized with regard to the square of the bunch width $2R/R_c$, which typically would be of the order of unity or smaller.

The curves in Figure 5.3 show that the perveance could be quite large if there were no restrictions on the deflection angle U. However, a number of additional constraints on U, to be discussed in the next section, put an upper limit on U_{max}. Hence, the perveance will always be fairly low, except at extreme relativistic velocities, where the situation clearly is more favorable.

As a typical, fairly low voltage design let us assume that $V_0 = 90$ kV and the bunch width $2R/R_c = 0.5$, and determine the maximum perveance and beam power for a few typical deflection angles $U \leq 0.5$. The data are listed in Table 5.1.

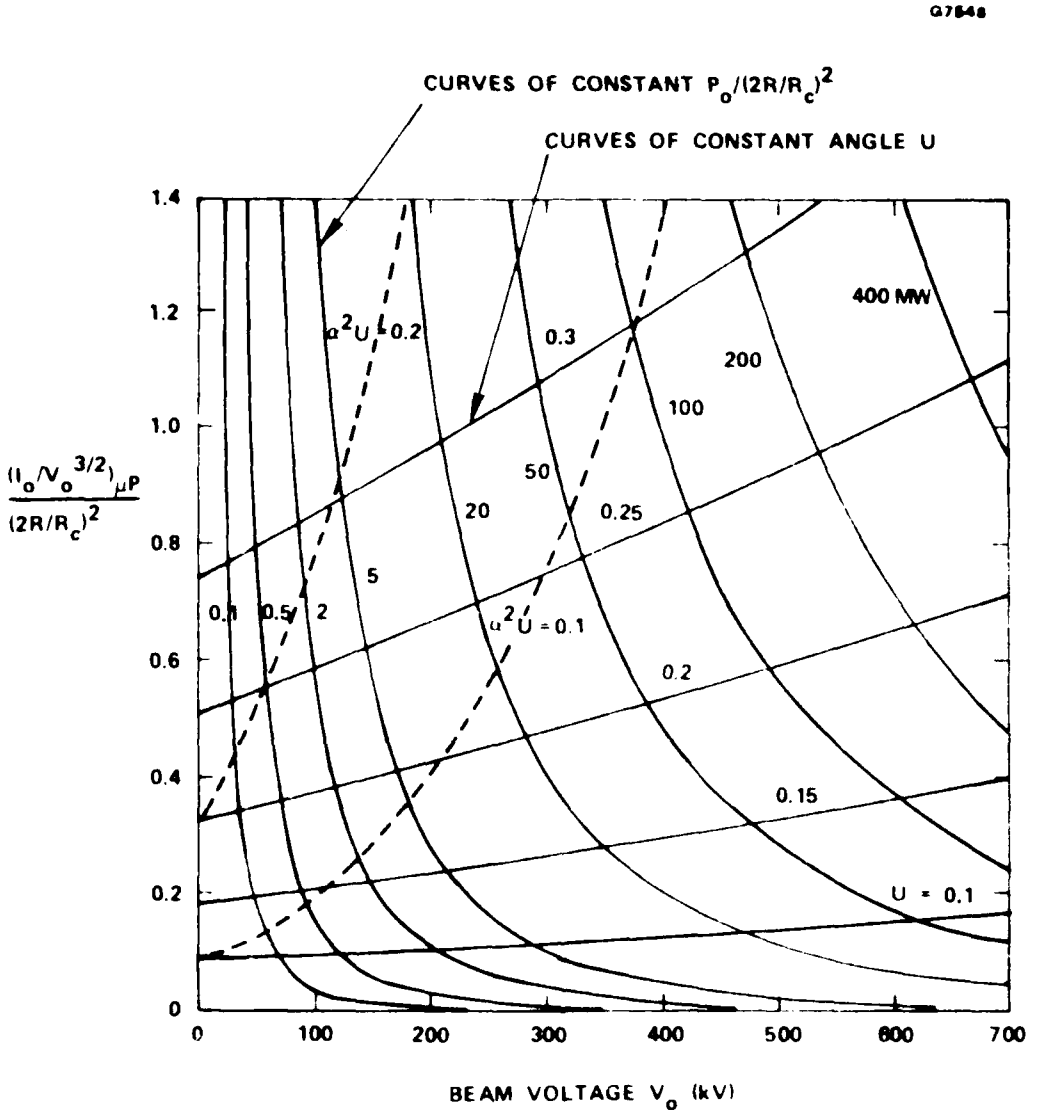

Figure 5.3 Universal design curves for the deflection modulated amplifier. The variables have the following significance:

$(I_0/V_0^{3/2})_{\mu P}$ = maximum microperveance

$2R/R_c$ = bunch width in radians at the output

U = deflection angle in radians

V_0 = dc voltage in kV

P_0 = dc beam power in MW.

TABLE 5.1

MAXIMUM PERVEANCE AND BEAM POWER FOR TYPICAL DEFLECTION ANGLES. VOLTAGE V_0 = 90 kV, BUNCH WIDTH $2R/R_c$ = 0.5 RADIAN

Deflection Angle, U	Maximum Perveance $I_0/V_0^{3/2}$	Maximum Beam Power
0.2	0.09×10^{-6}	240 kW
0.3	0.20×10^{-6}	490 kW
0.4	0.36×10^{-6}	880 kW
0.5	0.55×10^{-6}	1340 kW

At small deflection angles the perveance is fairly low. It increases as the square of both the angle and the bunch width. With an azimuthal bunch width of one half radian, the gyrocon compares very favorably with klystrons for which the corresponding phase may be four times as large. It should also be noted that the RF focusing effect in the gyrocon may further improve conditions by reducing the actual azimuthal bunch width. One might therefore consider designing with a larger bunch width to increase the perveance. On the other hand, the radial width of the bunch also has some constraints. These are related to the output ring resonator design and the need to provide a relatively constant RF retarding voltage over the radial extent of the bunch for efficient energy conversion. Accordingly, the data in Table 5.1 will be considered representative of the maximum practical perveance values for the deflection modulated amplifier at fairly low dc voltages.

5.2 LIMITATIONS ON DEFLECTION ANGLE

A large deflection angle leads to several kinds of problems, which can be stated as follows:

1. The beam distortion and RF focusing effects described in Section 4.2 increase with the product $\alpha^2 U$ and may become excessive. (An example is shown in Figure 7.5.)

2. The associated longitudinal velocity spread specified in (4.11) increaes with $\alpha^2 U$, and might lead to lower efficiency in the output resonator.

3. The transverse normalized displacement S_N at the exit of the last deflection cavity is typically 1.4 times the deflection angle, and might cause beam interception on the deflection plates.

All the three items are important in arriving at a compromise value of the deflection angle. By designing the last cavity with comparatively large transverse spacing of deflection plates, the interception problem might possibly be eliminated even with fairly large deflection angles. But we would still be faced with the increased beam distortion and longitudinal velocity spread. However, as noted earlier in Section 4.2, these effects are not proportional to U but to $\alpha^2 U$, and are therefore less serious at relativistic velocities. The two dotted curves in Figure 5.3 correspond to $\alpha^2 U = 0.1$ and $\alpha^2 U = 0.2$ and represent, in a sense, curves of constant RF distortion. Hence, from the point of view of distortion, these curves, whichever we choose as representative, introduce a limitation on the range of variables, which are not permitted to be <u>above</u> the curves $\alpha^2 U$ = constant. As noted earlier, and clearly evident from the dotted curves in Figure 5.3, the distortion rapidly becomes less of a limiting factor as the dc voltage is

increased into the relativistic domain. As an example, a 250 kV beam with microperveance 0.55 and deflection angle of 0.22 radians has basically the same RF distortion as a nonrelativistic low voltage beam with perveance 0.1 and deflection 0.1 radian. The example clearly shows that the device is expected to behave considerably better at high dc voltages.

The computer results discussed in Section 7 indicate that low voltage designs (90 kV) with U larger than 0.5 result in fairly large to excessive RF distortion effects. Hence, for this dc voltage we may conclude that U = 0.5 can be taken as a reasonable maximum value, whereas U = 0.3 probably is a better choice. From the data in Table 5.1, these two deflection angles correspond to an optimum microperveance of 0.55 and 0.2, respectively (assuming a bunch width of one half).

5.3 POSSIBLE HIGH FREQUENCY LIMITATION

The gyrocon has earlier been described as a low frequency device,[1-4] which cannot operate at high frequencies due to prohibitive beam size caused by space charge expansion. Apparently, these statements are based on misconceptions, because there is nothing in the more general present treatment that indicates an upper frequency limit beyond which operation is not possible. In fact, all the variables used in the theory are defined in their normalized form which implicitly contain the frequency as the product of frequency and length. This implies that all the dimensional parameters, such as length of deflection system, length of drift space, and beam size scale perfectly with frequency. An increase in frequency by a factor, say two, would merely require a corresponding reduction in all geometrical dimensions by a factor of two, including beam size. The relative beam expansion and the bunch width would be the same.

The only parameters which do not scale properly with frequency are the cavity losses, expressed by their Q-values, and thermal effects in the beam. The latter are not of major concern, while the reduction in cavity Q-values with frequency is not different from what happens in any microwave tube, such as klystrons and traveling-wave tubes. The loss problem and its role in determining a possible upper frequency limit are essentially the same in all such devices.

These considerations definitely apply for the deflection system of the present amplifier, and we may therefore conclude that there are no extraordinary frequency limiting factors for the deflection system of the amplifier beyond the usual loss problem having to do with getting sufficiently high Q-values in the cavities.

The output resonator, which is not treated in this first phase of the program, may introduce additional frequency limiting factors which will be mentioned only briefly. First, the required high efficiency of energy conversion, perhaps in the range of 90 percent, calls for a correspondingly high circuit efficiency, i.e., small internal cavity loss. And second, the power density and peak electric field allowable in the output gap put a limit on the minimum size of geometrical dimensions, and thereby on the upper frequency. Although these considerations are not at all unique for the deflection amplifier, the special traveling-wave resonator used in this device calls for a separate investigation of its frequency limiting factors. Before this is done we can only make the cautious statement that there are no apparent frequency limiting factors which are more serious than those found in any linear microwave tube, such as the klystron.

6.0 EXPERIMENTAL CAVITY STUDY

The objective of the experimental part of the study was to verify that cavity fields suitable for an electric deflection scheme in gyrocons could be achieved, and to measure the field characteristics. To date, gyrocons have been designed to operate with magnetic deflection. The deflection force is provided by a transverse magnetic field, established in a cavity that resonates in a pure TM mode. The cavity geometry is simple enough so that exact field solutions are available.

With electric deflection the cavity configuration is more complex. It has been shown[5] that a pure TE mode in a resonating cavity gives no net deflection.* Hence to accomplish electric deflection the field pattern cannot be pure TE. In practice this means a cavity with a non-uniform cross section for which analytical solutions seldom exist. Hence the need for experimental study.

6.1 GENERAL DESIGN CONSIDERATIONS

The deflection that is desired in a gyrocon may be illustrated by the operation of a cathode ray tube in an oscilloscope. The beam deflection is controlled by a transverse electric field set up by applying a voltage between two parallel plates. By having two deflection regions in succession, with the second rotated 90° relative to the first and driven 90° out of phase, a circular deflection pattern results. In a gyrocon the fields are set up by exciting a cavity resonance, rather than by applying a voltage between two electrodes. The frequency and power capabilities are then improved and power losses can be kept low.

*A transverse electric field necessarily goes to zero at each end of the cavity. The magnetic field associated with the spatially varying electric field exactly cancels the deflection due to the electric field. A transverse magnetic field, on the other hand, can remain constant in magnitude over the entire cavity length.

The following considerations were involved in the cavity designs:

1. Size of interaction region. During the traversal of an electron through the interaction region the time-varying field should change less than half a cycle or else the deflection force will reverse its sign. This condition is expressed by $\beta_e \ell < \pi$, where $\beta_e = 2\pi f/v_o$ and ℓ is the length of the interaction region. If the deflection in the two transverse directions is accomplished in separate cavities, it is possible to operate both cavities in phase provided the distance between their center planes, ℓ', satisfies the condition $\beta_e \ell' = \pi/2$. In practice this requires that $\beta_e \ell < \pi/2$ for each cavity. The transverse dimensions of the interaction region should be related to the beam size and lateral beam displacement. Assuming that the beam radius, r_b, is given by $\beta_e r_b \approx 0.2$, the plate separation d in the input deflection cavities was chosen as $\beta_e d \geq 1$.

2. Operating voltage. Gyrocons generally promise best performance at relatively high voltages, typically a couple of hundred kilovolts. For verifying cavity designs, however, the precise voltage is less important. Because the dimensions of the interaction region are proportional to the electron velocity, they change rather slowly with voltage at relativistic speeds. If the voltage is reduced from 200 kV to 80 kV, for example, the electron velocity decreases from 0.7 to 0.5 of the speed of light, or a drop of 30 percent. A nominal voltage of 80 kV was assumed for the initial cavity designs. This would be a suitable operating voltage for feasibility demonstration of an actual device. The experiments were planned in such a way

that the characteristics of cavities suitable for operation at higher voltages could also be estimated from the measured data.

3. Resonant frequency. For testing purposes, a nominal frequency of 1.5 GHz was chosen on the basis of convenient availability of test equipment and relatively large and easy-to-make cavity parts. By uniform scaling of all cavity dimensions, in inverse proportion to frequency, any other frequency can be obtained. Except for cavity losses, all pertinent field-energy relations are independent of cavity size. A uniform dimensional scaling also maintains constant operating voltage.

6.2 CAVITY TYPES AND DESCRIPTION OF EXPERIMENTS

As discussed in the preceding section, a particularly attractive design approach is an electron transit phase of $\pi/2$ between two successive parallel plate cavities with one rotated 90^{o} relative to the other. With a 80 kV beam and 1.5 GHz frequency, the desired distance between the center points of the two sets of plates is then 1.0 inches.

To get an initial idea of the cavity dimensions involved, one might consider a cylindrical cavity resonating in a TE_{111} mode. The general formula for the frequency of a TE resonance of order (mnp) in a cavity of length ℓ and radius a is[7]

$$\frac{f_{(mnp)}}{c} = \sqrt{\left(\frac{p}{2\ell}\right)^2 + \left(\frac{p'_{mn}}{2\pi a}\right)^2} \qquad (6.1)$$

Here p is the number of half sine-waves in the axial direction and p'_{mn} is the nth root of $J_m'(x) = dJ_m(x)/dx = 0$, with J_m being the mth order

Bessel function. In a TE resonance, the integer p has to be at least one. With $p'_{11} = 1.841$ and $\ell = 1.0$ inches it turns out that the frequency cannot be less than 5.9 GHz no matter how large the radius. Alternatively, the axial dimension cannot be less than 4 inches for a 1.5 GHz frequency.*

Although the actual deflection cavities are capacitively loaded in the middle, lowering the frequency, there was some doubt that suitable cavities with a short axial dimension could be obtained. It was consequently planned to also investigate longer cavities.

One of the limiting conditions in gyrocon design is the beam spread due to space charge, since for efficient energy conversion in the output resonator the beam cross section should be small. A single cavity that sustains a circularly polarized deflection field has the advantage of shorter total interaction length and therefore smaller beam spread. Such a field can be maintained in any resonating cavity with 90° rotation symmetry, if it is excited by couplers located 90° apart and driven 90° out of phase. Two such general cavity types were considered: a four-plate cavity, and a magnetron-type cavity. Figure 6.1 is a photograph of the main types that were evaluated.

As it turned out, the most attractive cavity was a composite of two parallel plate cavities in series, with internally connected plates. Figure 6.2 is a picture of such a cavity. The second set of plates is rotated 90° and the two sets are pairwise connected. The composite

*For a cavity resonating in a TM mode an equation similar to (6.1) holds, with p'_{mn} replaced by p_{mn}, the nth root of $J_m(x) = 0$. However, no axial variation is now required so that p can be zero. The frequency is then independent of ℓ. For the TM_{110} mode, with $p_{11} = 3.83$, the 1.5 GHz frequency requires a cavity diameter of 9.6 inches.

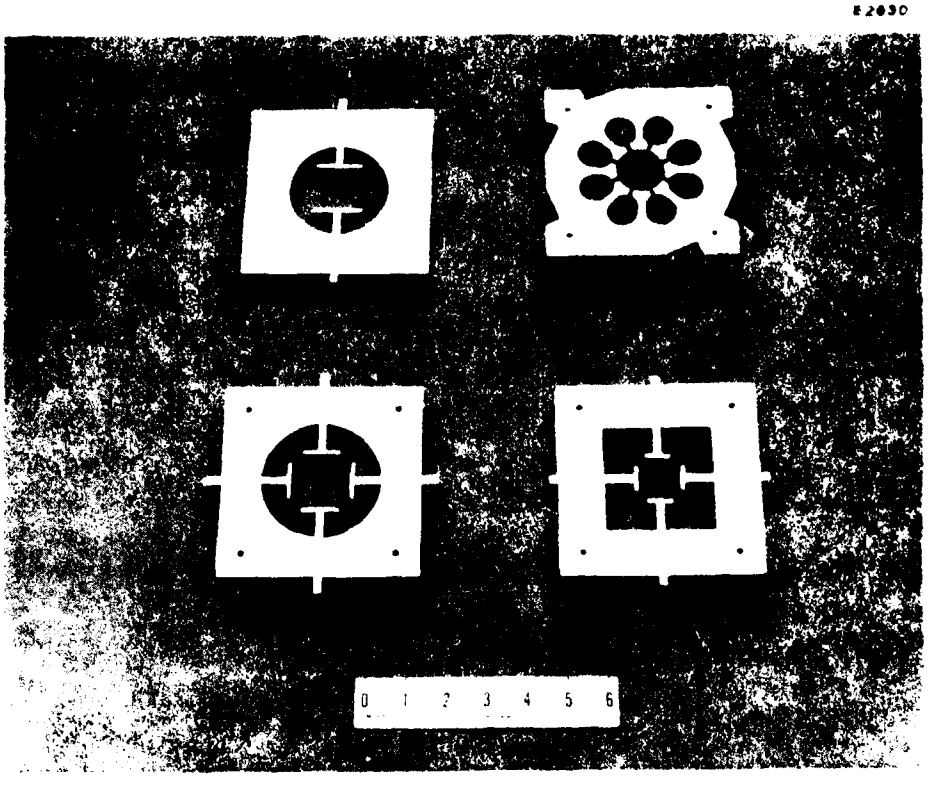

Figure 6.1 Main cavity types evaluated experimentally.

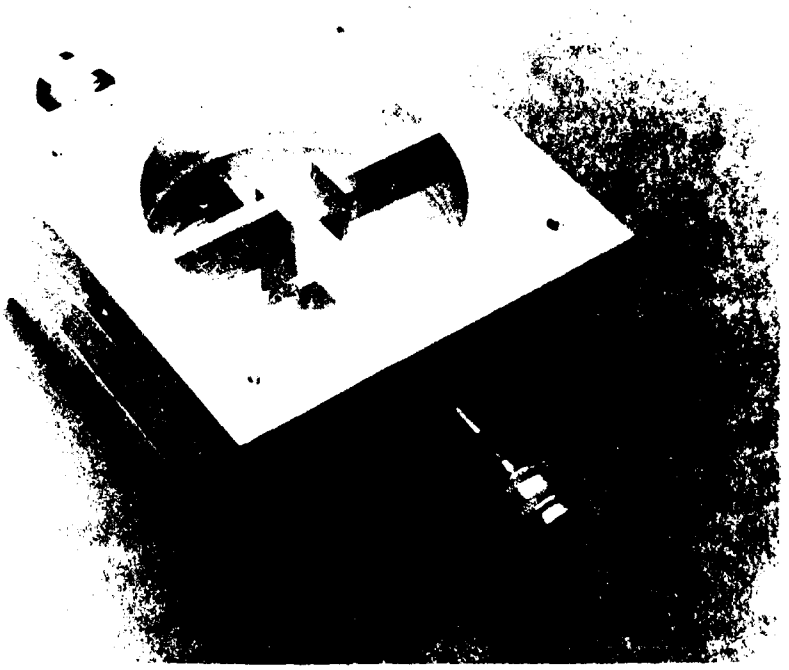

Figure 6.' Composite cavity with [illegible] laterally connected [illegible]

cavity, when operated at the correct beam voltage for a transit phase of $\pi/2$, provides a circularly deflected beam with a single input signal. It also has a high interaction impedance, giving a large deflection sensitivity.

Figure 6.3 defines the configuration of a parallel plate cavity. The plate assembly, indicated by the dimension ℓ_o, is sandwiched between two spacers and an endplate on either side. Holes are provided through the middle of the plates for field strength measurement by perturbation with a dielectric rod or small spherical bead. The field can likewise be probed along the other two principal axes. The cavity was usually excited by a small inductive loop near the base of the plate support, as may be seen in the photograph of Figure 6.2, although electric probe coupling was also possible.

The other cavity types were put together in a similar manner. Figure 6.4 is an exploded view of the assembly of a four-plate cavity. Most of the parts could be used in either a two-plate or a four-plate configuration. Changes could be made in several cavity dimensions by part substitution. Variable plate separation was allowed by slots in the plate supports.

The detailed configuration of the magnetron cavity, with major dimensions indicated, is presented in Figure 6.5. The part was modified once to lower the frequency response by machining out the circular channels as shown. Due to the variety of modes possible in this type of cavity a more elaborate provision was made for probing the fields. The different axes and the location of the inductive loop couplers are also indicated in the figure. Some laterally displaced holes parallel to two of the axes were included to make it possible to short out some otherwise degenerate field patterns with a metal wire.

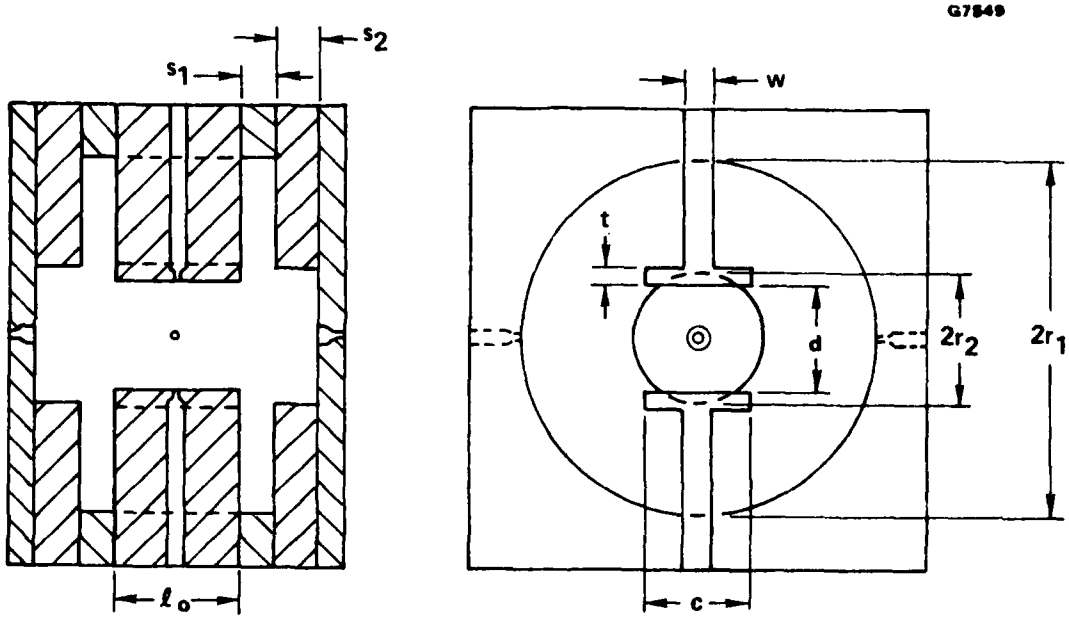

Figure 6.3 Configuration of two-plate cavity with definition of dimensional parameters.

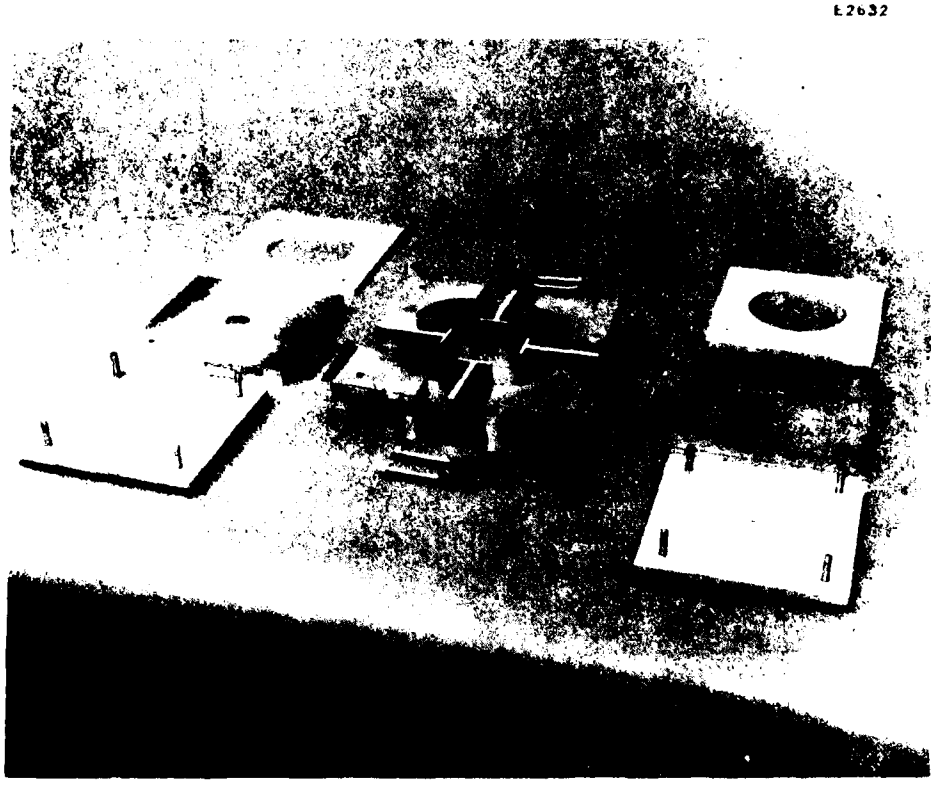

Figure 6.4 Exploded view of the parts of a four-plate cavity.

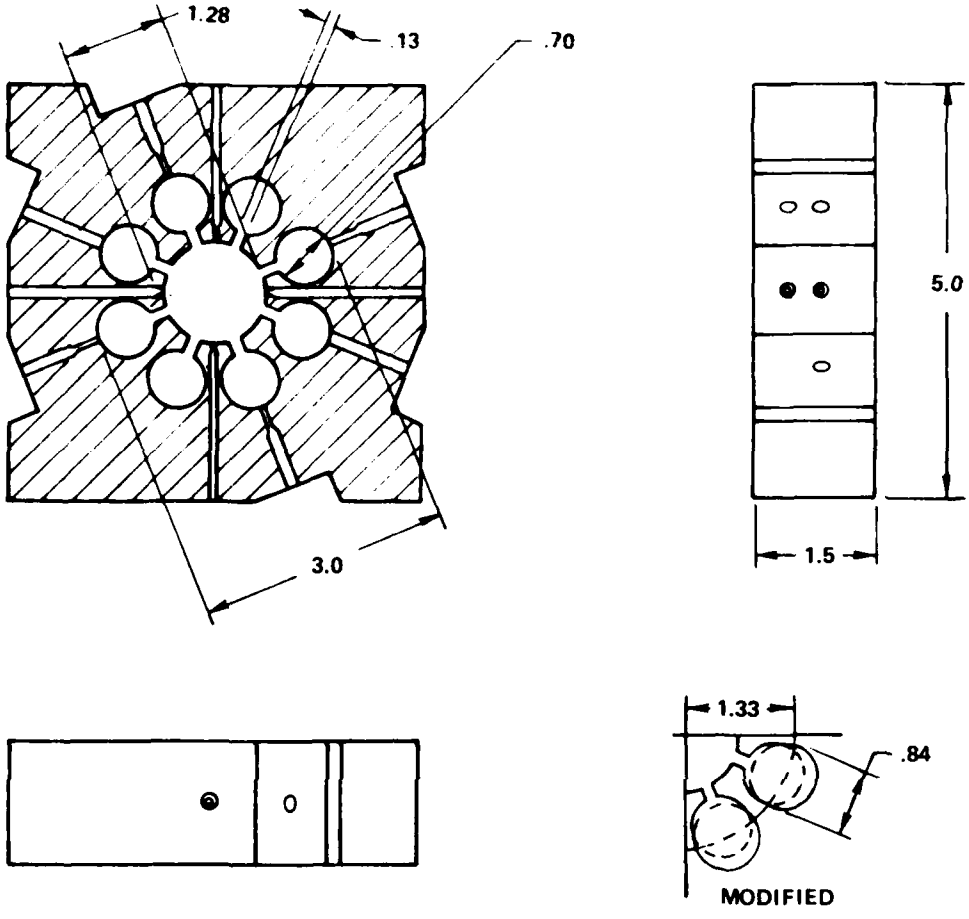

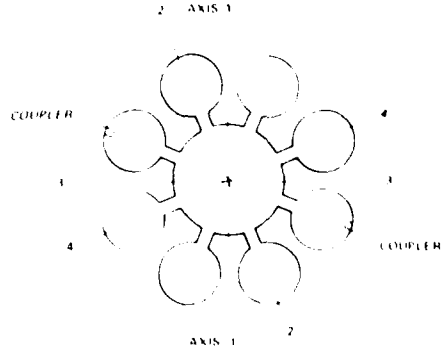

Figure 6.5 Configuration of the magnetron-type cavity and axes for field probing.

All the cavity parts were made of aluminum for easy machineability. The use of aluminum and a structure that was clamped together did not provide for a meaningful measurement of the intrinsic cavity loss, but accurate loss information was not considered essential for the study of the input and deflection cavities. For general information, the Q of the coupler-cavity system was measured by noting the resonance width. Typical values ranged from 500 to 1000. The resonance widths were often fairly sensitive to clamping pressure.

The major electrical properties to be determined for a given cavity were its resonant frequency and interaction impedance. The impedance relates the square of the electric field strength to the total energy in the cavity. It was measured by perturbing the cavity with a dielectric rod along the (approximately uniform) transverse electric field. The standard perturbation relation between the frequency shift and field strength is given in Appendix B.

For an accurate evaluation of the deflection properties of a cavity one would also need to know the variation of the fields along the beam trajectory. Perturbation measurements with dielectric and metal beads makes it possible, in principle, to determine the magnitude of both the electric and magnetic fields as a function of position. The perturbation formulas for small spherical beads are presented in Appendix B. A dielectric bead perturbs only the electric field while a metal bead affects both. To determine the magnetic field strength in a region where electric field is also present requires taking the difference between the frequency shifts observed with the two beads. In practice the shifts involved were small, typically 1 MHz or less. Profiles of electric deflection fields could often be established reasonably well, but the magnetic field throughout the deflection region was not measurable due to the large uncertainty associated with subtracting two shifts of similar magnitude.

6.3 EXPERIMENTAL DATA

6.3.1 Parallel Plate Cavity

The basic parallel plate cavity was measured for a number of different configurations. One of these had a resonant frequency of 1.505 GHz, which is very close to the nominal design value of 1.5 GHz. The relevant data are listed in Table 6.1, where the dimensional parameters are as defined in Figure 6.3.

TABLE 6.1

DIMENSIONS AND DATA ON PARALLEL PLATE REFERENCE CAVITY

Cavity Dimension	Inches	
d	.64	Frequency, f = 1.505 GHz
ℓ_o	.80	Frequency shift, Δf = -8.0 MHz
c	.64	Rod diameter, $2r_d$ = .0635"
t	.10	Dielectric const., $\varepsilon/\varepsilon_o$ = 9.0
w	.20	Field strength, $\varepsilon_o\langle E^2\rangle/W$ = 1.31 in^{-3}
s_1	.20	Field at center, $E_o^2/\langle E^2\rangle$ = 0.92
$2r_1$	3.50	
s_2	.20	$\left(\frac{R}{Q}\right)_{\ell_o} = \frac{E_o^2 \ell_o^2}{2\omega W} = 182\ \Omega$
$2r_2$	.74	

The perturbing rod establishes the field-to-energy ratio $\langle E^2 \rangle / W$, where $\langle E^2 \rangle$ is the average value of the electric field squared between the plates and W is the total energy in the cavity. The field variation between the plates was measured by bead perturbation. From this the field at the center, E_o, could be determined. Typically $E_o^2 / \langle E^2 \rangle = .92$ (as in the example shown in Figure 6.9 in Section 6.3.2). For comparison purposes a parameter $(R/Q)_{\ell_o}$ was defined by

$$\left(\frac{R}{Q}\right)_{\ell_o} = \frac{E_o^2 \, \ell_o^2}{2\omega W} \tag{6.2}$$

This would be the R/Q - parameter involved in the interaction, if the field E_o was maintained over the distance ℓ_o. Actually the field drops off from its value at the center and extends over a larger region. The values used in the calculations of the deflection system performance were therefore corrected (Section 7).

Figures 6.6 and 6.7 illustrate how the frequency and the ratio $\varepsilon_o \langle E^2 \rangle / W$ change as the cavity dimensions are varied from those of the reference cavity. The data points in each case represent a specific measured cavity configuration. Of particular interest is the case when both the plate separation d and the plate width c are simultaneously increased, with d = c, while everything else is kept the same. The data show that the frequency stays practically constant, while the impedance, or R/Q, decreases rapidly with the size of the deflection region. It is therefore very desirable to keep the size small, within the constraints imposed by the size and behavior of the deflected electron beam. A second feature to be noted is the drop in impedance with decreasing spacer thickness s_1. It results from the increased electric energy between each plate and the shorting plane at the ends, representing energy that is not useful for the deflection.

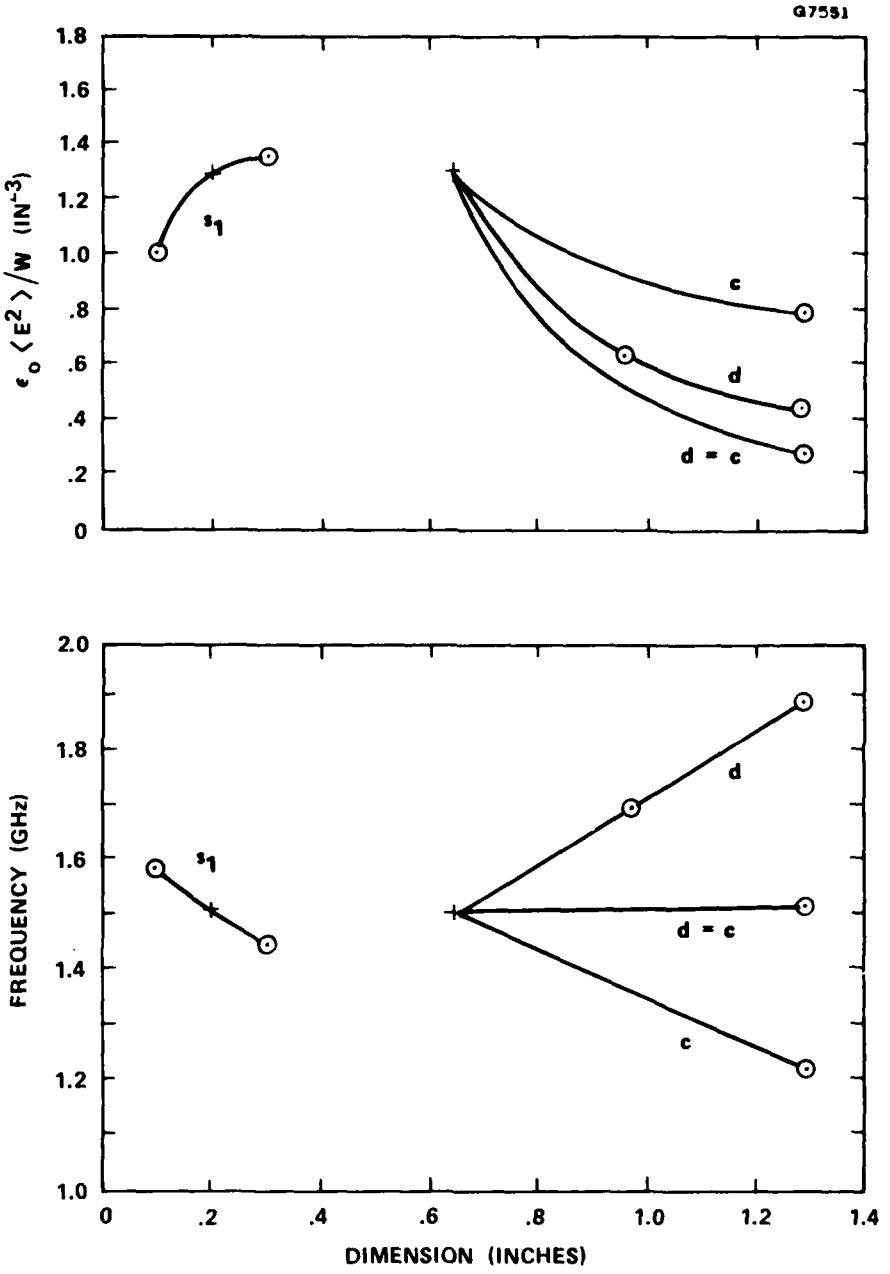

Figure 6.6 Change in frequency and impedance, $\epsilon_o \langle E^2 \rangle / W$, with plate dimensions and spacer thickness. The reference cavity of Table 6.1 is represented by the cross symbol.

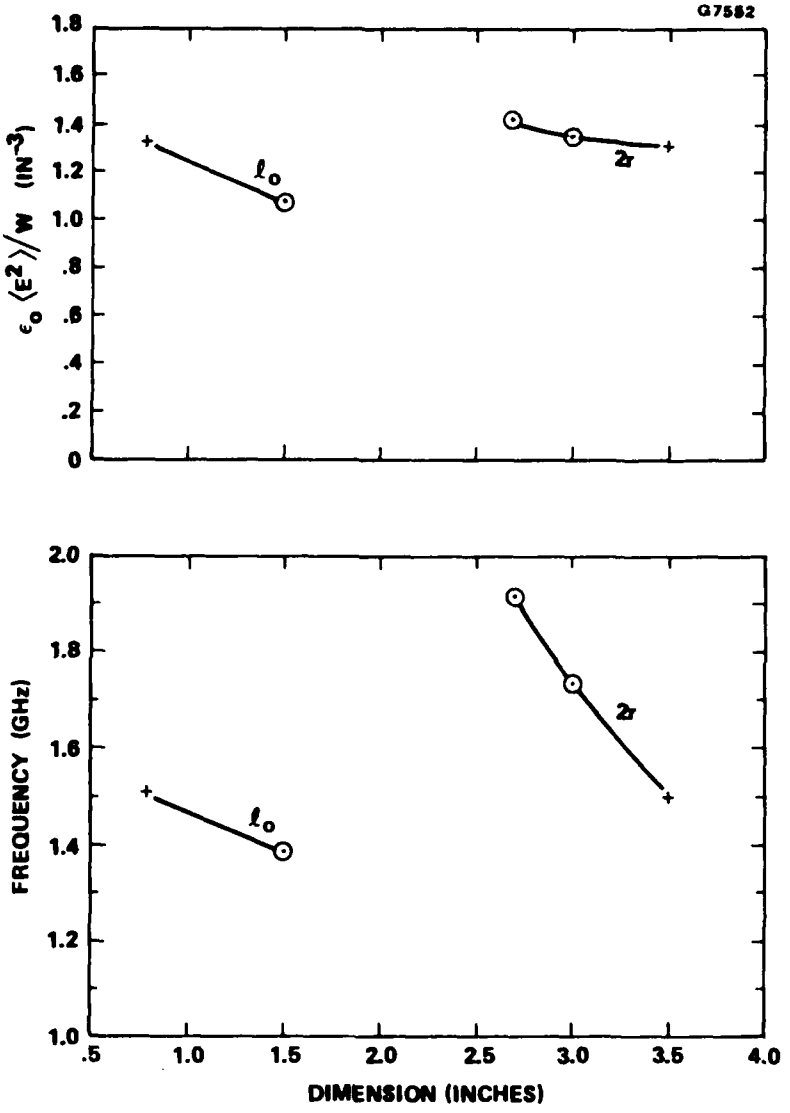

Figure 6.7 Change in frequency and impedance, $\epsilon_o \langle E^2 \rangle / W$, with plate length and cavity diameter. The reference cavity of Table 6.1 is represented by the cross symbol.

The reference cavity was designed for an 80 kV beam. A larger voltage means a longer cavity as well as a larger deflection region. Using data taken with a plate length ℓ_o of 1.5 inches and making a number of interpolations, the cavity characteristics at 150 kV and 280 kV could be estimated. As before, the following assumptions were made:

$$\beta_e (\ell_o + s_1) = \pi/2 \tag{6.3}$$

$$\beta_e d = 1.0 \tag{6.4}$$

$$c = d \tag{6.5}$$

For convenience, the spacer thickness s_1 was kept fixed at .20 inches, while the cavity frequency was maintained at 1.5 GHz. The results are summarized in Figure 6.8. Both the R/Q - parameter and the cavity diameter decrease rather slowly with voltage.

6.3.2 Composite Parallel Plate Cavity

The composite parallel plate cavity has been described in Section 6.2. Its resonant frequency is generally lower than the frequency of a similar single cavity. With the single cavity dimensions as given in Table 6.1, and a central cavity spacer with thickness s_o = .20 inches and iris diameter $2r_o$ = 3.5 inches, the frequency of the composite cavity was 1.383 GHz compared to 1.505 GHz for the single cavity.

The frequency can be raised in several ways. The best approach would be to reduce the main cavity diameter, to an estimated 3.2 inches. However, availability of parts made it more convenient to modify spacer dimensions instead. Without changing the geometry of the main deflection region, the frequency could be increased to 1.452 GHz by reducing

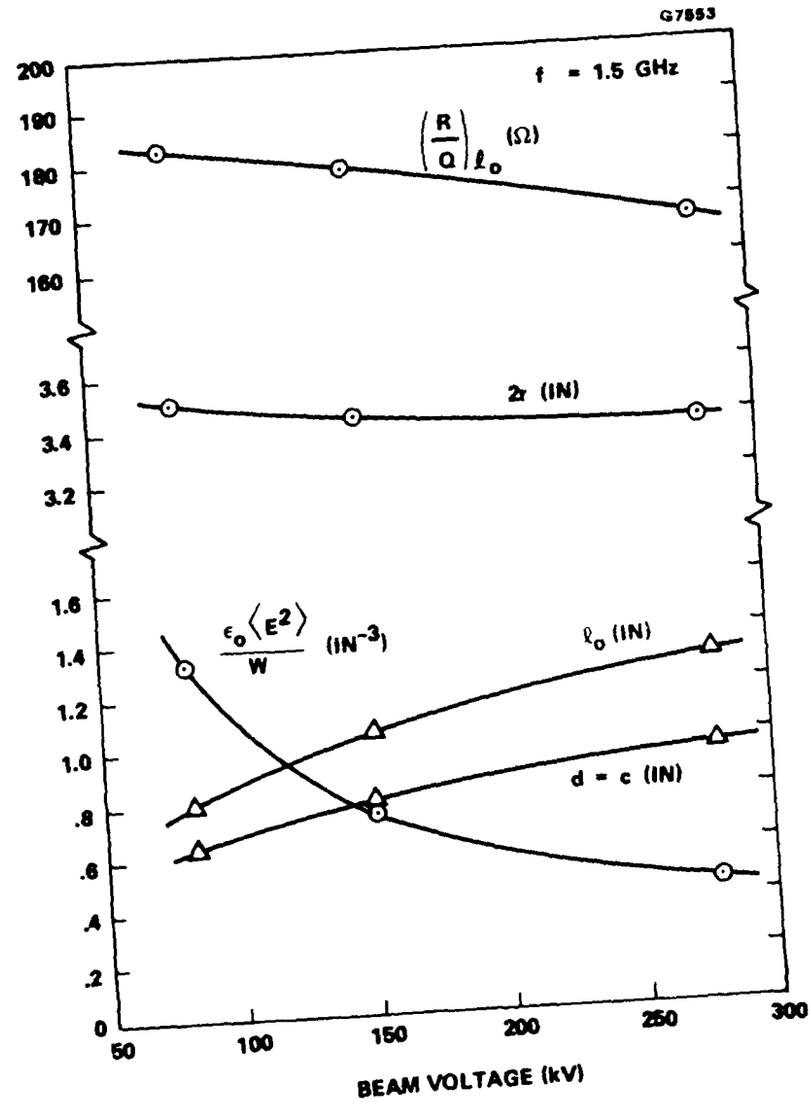

Figure 6.8 Parameters of parallel plate cavity vs voltage.

the thickness s_1 of the end spacers from .20 to .10 inches, and to 1.493 GHz by also decreasing the iris diameter to 3.0 inches.

The characteristics of the last configuration are summarized in Table 6.2. The value of R/Q is smaller by a factor of two relative to the value in a single cavity, only because the total energy is twice as large. The effectiveness of the composite cavity is as good as that of two uncoupled cavities, because in the latter case both cavities would require an input signal, resulting in the same total drive power.

TABLE 6.2

CHARACTERISTICS OF COMPOSITE PARALLEL PLATE CAVITY.
(Dimensions the same as in reference cavity, Table 6.1, except as noted.)

End spacer thickness, s_1 = .10"
Central spacer thickness, s_o = .20"
Central iris diameter, $2r_o$ = 3.0"
Frequency, f = 1.493 GHz
Frequency shift, Δf = -4.0 MHz
Rod diameter, $2r_d$ = .0635"
Dielectric const., $\varepsilon/\varepsilon_o$ = 9.0
Field strength, $\varepsilon_o\langle E^2\rangle/W = 0.66\ in^{-3}$
Field at center, $E_o^2/\langle E^2\rangle = 0.92$
$(R/Q)_{\ell_o} = 92\ \Omega$

Electric field profiles, in the composite cavity defined in Table 6.2, are displayed in Figures 6.9 and 6.10. The profiles along the transverse directions, Figure 6.9, are essentially the same that one would measure in a single parallel plate cavity. Close to a metal surface the perturbation formula is not applicable. This makes it necessary to guess the field variation near the plates in the lower half of the figure. Figure 6.10 shows the profiles along the z axis. What is measured with a dielectric bead is the square of the total electric field. Invoking symmetry and requiring that $E_x^2 + E_y^2 = E^2$ allows one to determine E_x^2 and E_y^2 individually with reasonable confidence.

The composite cavity that was measured would be suitable for operation at 80 kV. Using the data in Figure 6.8 it is evidently possible to determine the expected characteristics at higher voltages as well. In particular, the parameter $(R/Q)_{\ell_o}$ would be just one half of the value that is plotted for the single parallel plate cavity.

6.3.3 Four-Plate Cavity

Figure 6.11 presents a comparison between a two-plate cavity and a four-plate cavity. Both cavities operate at nearly the same frequency and have the same length of deflection region. They also have the same cavity diameter, although this is not essential for the present comparison as long as the frequencies are the same. (The two-plate cavity is represented in Figure 6.7 by the data points at 2r = 3.0 inches.) It is evident from the field patterns in the figure that to maintain a similar degree of uniformity in field strength over a given deflection region, it is necessary to increase the plate separation in the four-plate cavity, since at the side plates the relevant field component goes to zero. Hence the plate separation has been increased by 50 percent while the plate width is the same. As a result, the

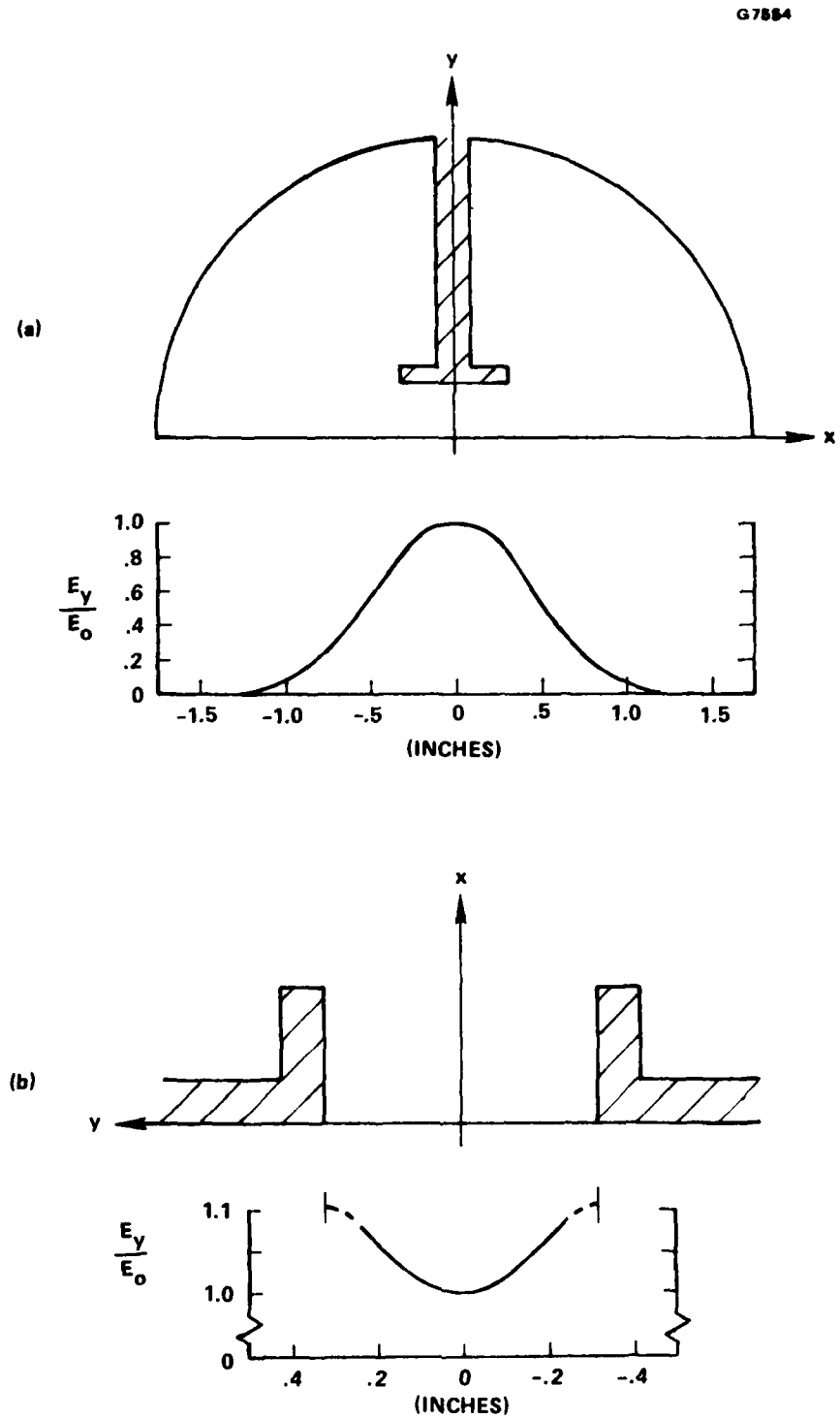

Figure 6.9 Electric field profiles along the transverse axes between the plates in a composite cavity.
a) Along x axis
b) Along y axis

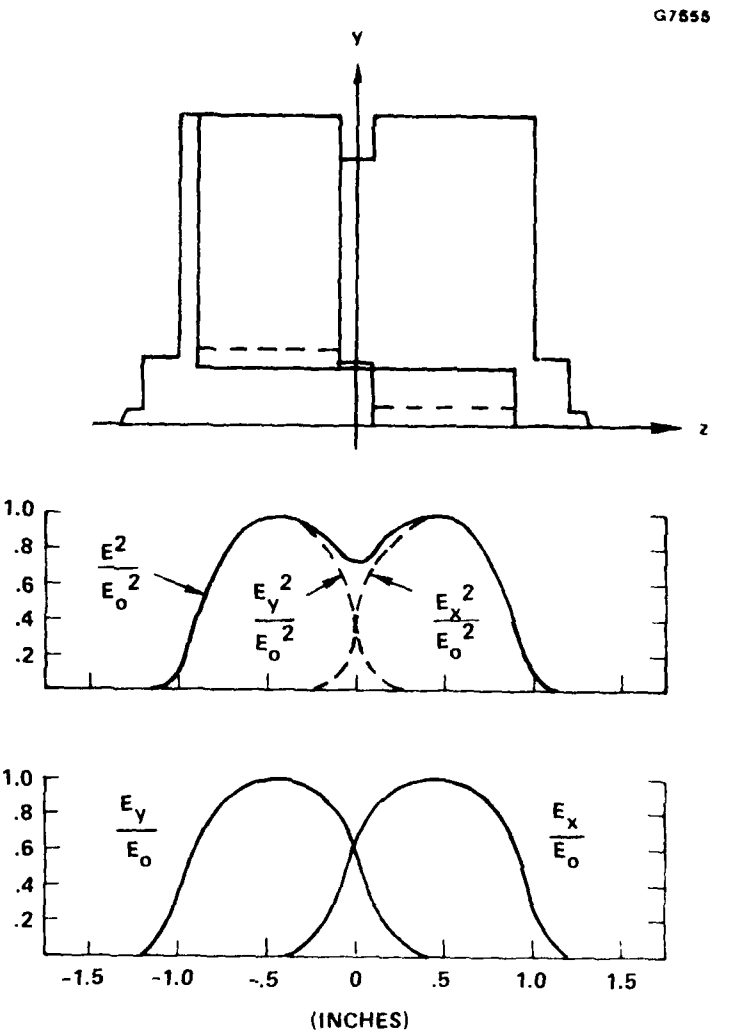

Figure 6.10 Electric field profiles along the longitudinal axis in a composite cavity.

G7886

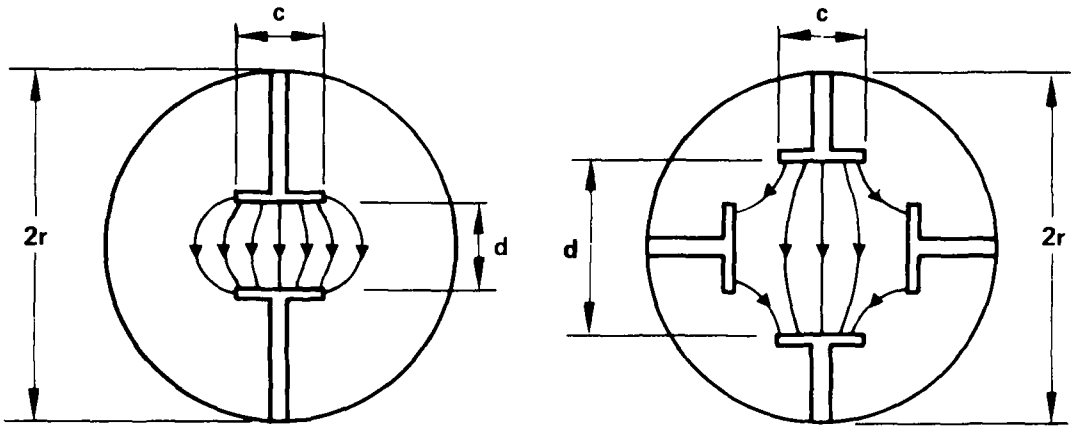

CAVITY TYPE	TWO-PLATE	FOUR-PLATE
2r	3.0 "	3.0 "
c	.64"	.64"
d	.64"	.96"
ℓ_o	.80"	.80"
s_1	.20"	.20"
f	1.738 GHz	1.773 GHz
Δf	-9.5 MHz	-4.0 MHz
$\varepsilon_o\langle E^2\rangle/W$	1.35 in^{-3}	.37 in^{-3}
$(R/Q)_{\ell_o}$	162Ω	44Ω

Figure 6.11 Comparison of a two-plate and a four-plate cavity.

deflection field in the four-plate cavity is significantly reduced, with an R/Q of less than 30 percent of that in the two-plate cavity.

A comparison between cavities of square and circular cross section (Figure 6.1) revealed no significant advantage of one type over the other. To get the same resonant frequencies with given internal plate configuration, the cross-sectional area of the square cavity had to be 10-20 percent larger. This is expected to be true for two-plate cavities also. For an actual operating device the method of cavity construction, and the overall cavity size, i.e., operating frequency, is likely to determine the choice of configuration.

6.3.4 Magnetron-Type Cavity

For the magnetron-type cavity, the central plate assembly in the two-plate cavity, shown in Figure 6.3 as extending over the length ℓ_o, was replaced by the part in Figure 6.5. The initial configuration, with magnetic loop coupling, exhibited four resonances in the range 2.02-2.24 GHz and a fifth resonance at 4.05 GHz. To lower the frequencies the peripheral holes were enlarged as detailed in Figure 6.5. The results are listed in Table 6.3.

The mode designation in the table is defined in Figure 6.12, where the arrows represent electric field lines and the circles with a cross or a dot inside represent magnetic field lines going into or coming out of the plane of the paper. A time difference of a quarter of a cycle also exists between the electric and magnetic lines.

For gyrocon operation the mode of interest is the dipole-like mode A. In the present cavity it occurred at 1.911 GHz, higher than the octupole mode of type D. The latter evidently has a phase shift of π between adjacent gaps and is referred to as the π-mode in magnetron theory.[8]

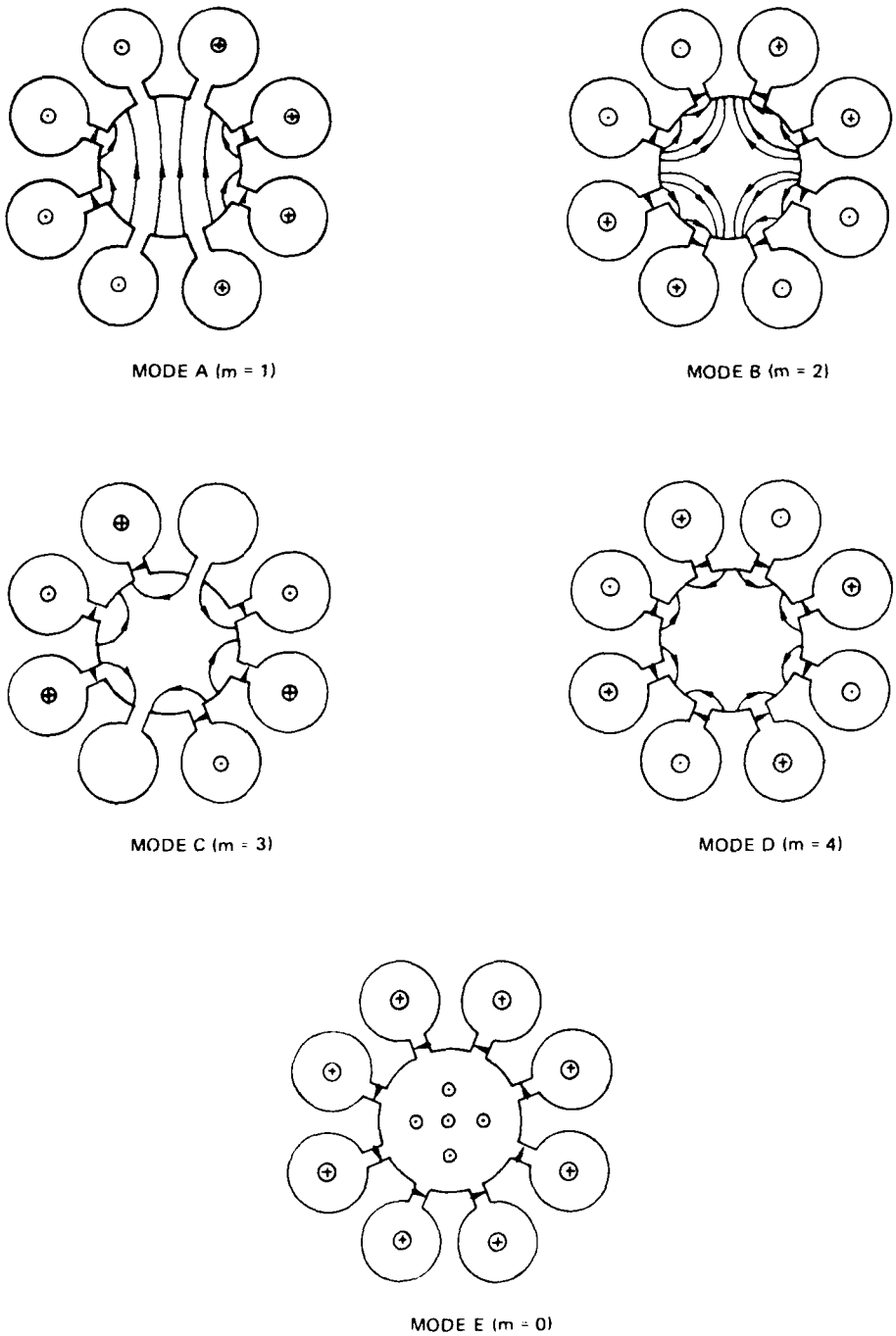

Figure 6.12 Some resonance modes in the magnetron-type cavity. The gross field variation with angle is given by the mode number m through a factor $e^{-jm\theta}$.

TABLE 6.3

DATA ON THE MODIFIED MAGNETRON-TYPE CAVITY WITH MAGNETIC LOOP COUPLING.

Spacer Dimensions: $s_1 = 0.20''$, $2r_1 = 3.50''$
$s_2 = 0.50''$, $2r_2 = 1.38''$

Dielectric Rod Data: $2r_d = 0.0635''$, $\epsilon/\epsilon_o = 9.0$

Frequency (GHz)	Frequency Shift[a] (MHz)	Mode	Degenerate
1.607	-0.5	D	No
1.631	-2.5; 0	C	Yes
1.716	-2.5; 0	B	Yes
1.911	-5.0; 0	A	Yes
3.828	0	E	No

[a]Rod along Axis 1.

Mode D is distinguished from modes A, B, and C by being nondegenerate. In the table this is indicated by a single frequency shift with dielectric rod. (In a doubly degenerate mode the resonance generally splits up into two when perturbed.) The nondegeneracy of the lowest frequency plus the large frequency shift of the fourth resonance help to identify the modes as shown in the table. In standard magnetron cavities the dipole resonance is frequently lowest. One cause for the reversal is the presence of a cylindrical electrode at the center of the magnetron. This tends to lower the frequencies by the increased capacitance. Because the dipole mode is the only mode with non-zero electric field on the axis, it is shifted more than any of the others.

The highest resonance, at 3.828 GHz and also nondegenerate, was characterized by a positive frequency shift when perturbed with a metal bead. It therefore had magnetic field along the axis and was identified as mode E.

With an interaction region length of ℓ_o = 1.5 inches and a frequency of 1.911 GHz, the measured magnetron-type cavity does not have the desired properties for a deflection cavity. We may still compare it to an equivalent two-plate cavity to get some idea of its potential effectiveness. Starting from a measured configuration, Case 1 in Table 6.4, the properties of an equivalent configuration, Case 3, have been estimated, using as a guide the variations plotted in Figures 6.6 and 6.7. The resulting interaction strength parameter, $\varepsilon_o \langle E^2 \rangle / W$, is about 20 percent

TABLE 6.4

COMPARISON BETWEEN THE MAGNETRON-TYPE CAVITY AND SOME TWO-PLATE CAVITIES

Parameter	Two-Plate Cavity			Magnetron-Type Cavity
	Case 1	Case 2[a]	Case 3[a]	
ℓ_o (in)	1.5	1.5	1.5	1.5
d (in)	0.96[b]	1.28[b]	1.28[b]	1.28[c]
2r (in)	3.0	3.0	2.6	(3.5)
f (GHz)	1.655	1.67	1.91	1.911
Δf (MHz)	-5.5	-	-	-5.0
$\frac{\varepsilon_o \langle E^2 \rangle}{W}$ (in^{-3})	0.55	0.33	0.38	0.32

[a] Frequency and $\varepsilon_o \langle E^2 \rangle / W$ estimated
[b] For the two-plate cavity, c = d
[c] For the magnetron-type cavity, d is a diameter

larger for the equivalent two-plate cavity than for the magnetron-type cavity. The difference is not considered very significant. The fact that the magnetron-type cavity can sustain a true circularly polarized mode may make it an attractive alternative for the floating deflection cavities. This is particularly true in situations where it is important to keep the total interaction length small to avoid excessive beam expansion.

Although the frequency measured for this particular magnetron-type cavity was too high for a deflection cavity (with the given dimensions of the deflection region), no difficulty is forseen in achieving a required resonance frequency by enlarging the peripheral holes. The cavity size will generally be larger than that of an equivalent two-plate cavity.

7.0 TYPICAL PERFORMANCE OF MULTICAVITY DEFLECTION SYSTEMS

We shall now present the main results of a few computer runs, in an effort to demonstrate the basic performance of multicavity deflection systems.

All these examples assume the double parallel plate cavity, with the following data:

Normalized length of each plate set = $0.4\ \pi$
Normalized separation between cavities = $0.05\ \pi$
Characteristic impedance R_{sh}/Q = 70 ohms

These data are consistent with the experimental cold test measurements. The value of $(R/Q)_{\ell_o}$ = 92 ohms in Table 6.2 has been reduced to 70 ohms to account for the variation of the transverse electric deflection field along the longitudinal axis. The Q-value was not experimentally established, except that it could be at least 1000; in the analysis the cavity Q is therefore taken as an adjustable parameter.

We are predominantly interested in the RF gain of the multicavity deflection system, and the size and shape of the beam cross section at the position of the output cavity. All the results refer to a bunch width of 0.5 radian, i.e., the ratio $2R/R_c$ is equal to 0.5. The normalized beam radius at the beam minimum is generally assumed to be $R_o = 0.25$, and the normalized radius of the output resonator is therefore $R_c = 2$.

Although the computer program can handle any number of deflection cavities, the gain very quickly becomes excessively high if the number exceeds three. Therefore, we shall limit ourselves to three cavities.

Taking the nominal RF output power equal to the dc power P_c (meaning essentially 100 percent efficiency), the power gain is defined by the ratio P_o/P_i, where P_i is the RF input power. The input power is the power required to cause a beam deflection of U radians at the exit of the particular cavity considered.

7.1 RF GAIN IN THE THREE-CAVITY DEFLECTION SYSTEM

Table 7.1 presents the calculated gain for the four optimum design conditions listed earlier in Table 5.1. The beam voltage is 90 kV and the bunch width is taken to be 0.5 radian, the same as in Table 5.1. The unloaded Q-value is 5000 for all three cavities, and all the cavities are tuned to resonance.

The additional gain per stage is quite high, roughly 15 dB, 18 dB, 20 dB, and 22 dB for the four cases, respectively.

The corresponding beam cross sections at the position of the output cavity are plotted in Figures 7.1 and 7.2. The actual cross sections are non-circular. The dotted straight lines through the beam center indicate the direction to the tube axis. The inner dotted circle is the dc beam size at the beam minimum, presumably located at the exit of the deflection system. The outer dotted circle is the dc beam size at the location of the output cavity.

TABLE 7.1

POWER GAIN OF THE FOUR CASES LISTED IN TABLE 5.1

Case	Deflection Angle U (radians)	Beam Perveance ($\mu A/V^{3/2}$)	Beam Power (kW)	Power Gain (dB)		
				Cavity 1	Cavity 2	Cavity 3
1	0.2	0.09	240	13.3	27.0	41.2
2	0.3	0.20	490	11.8	29.3	47.0
3	0.4	0.36	880	10.6	30.6	50.7
4	0.5	0.55	1340	9.3	30.7	52.1

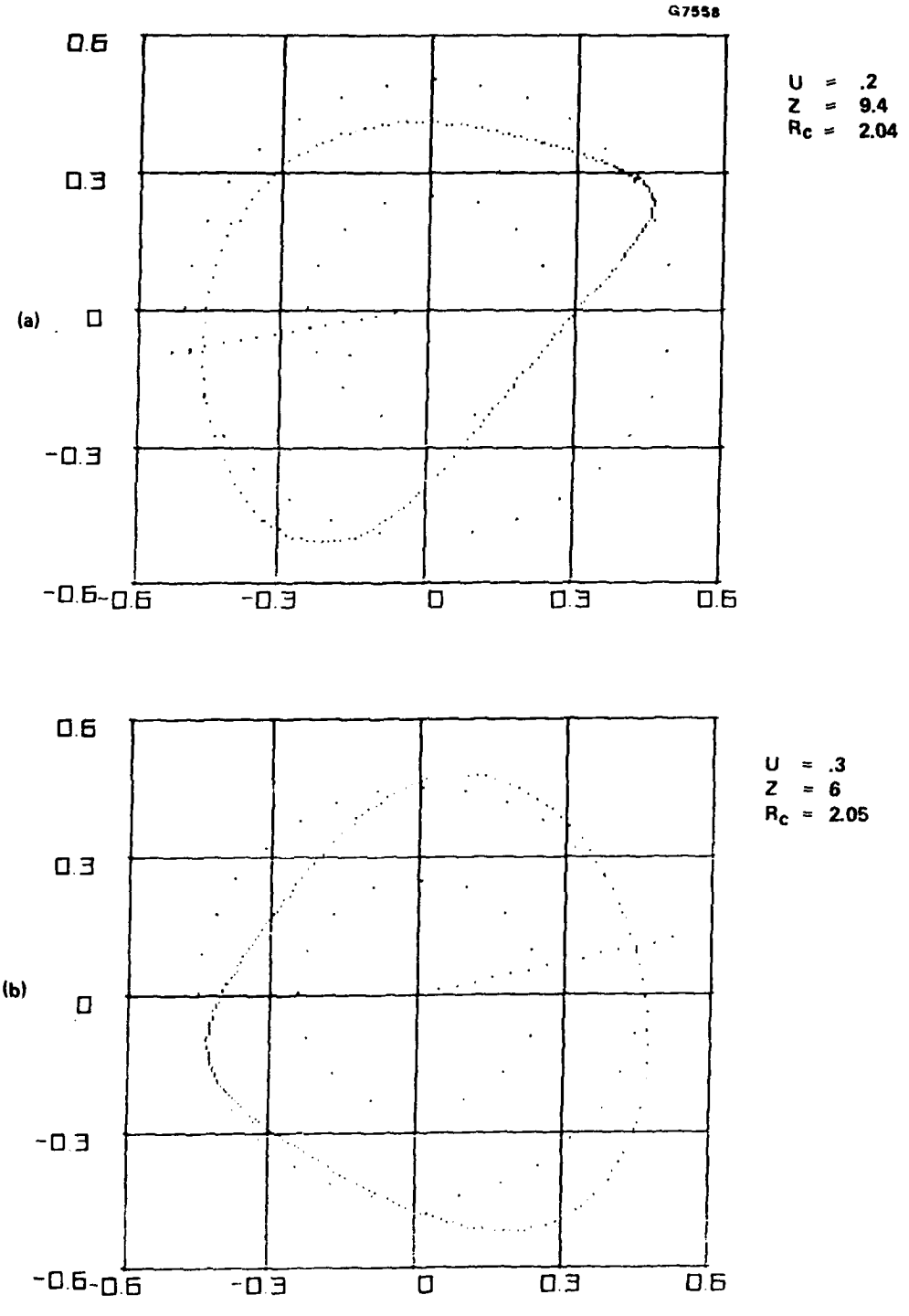

Figure 7.1 Beam cross sections at the position of the output resonator for the first two cases listed in Table 7.1.
a) $U = 0.2$, perveance = 0.1×10^{-6}
b) $U = 0.3$, perveance = 0.2×10^{-6}

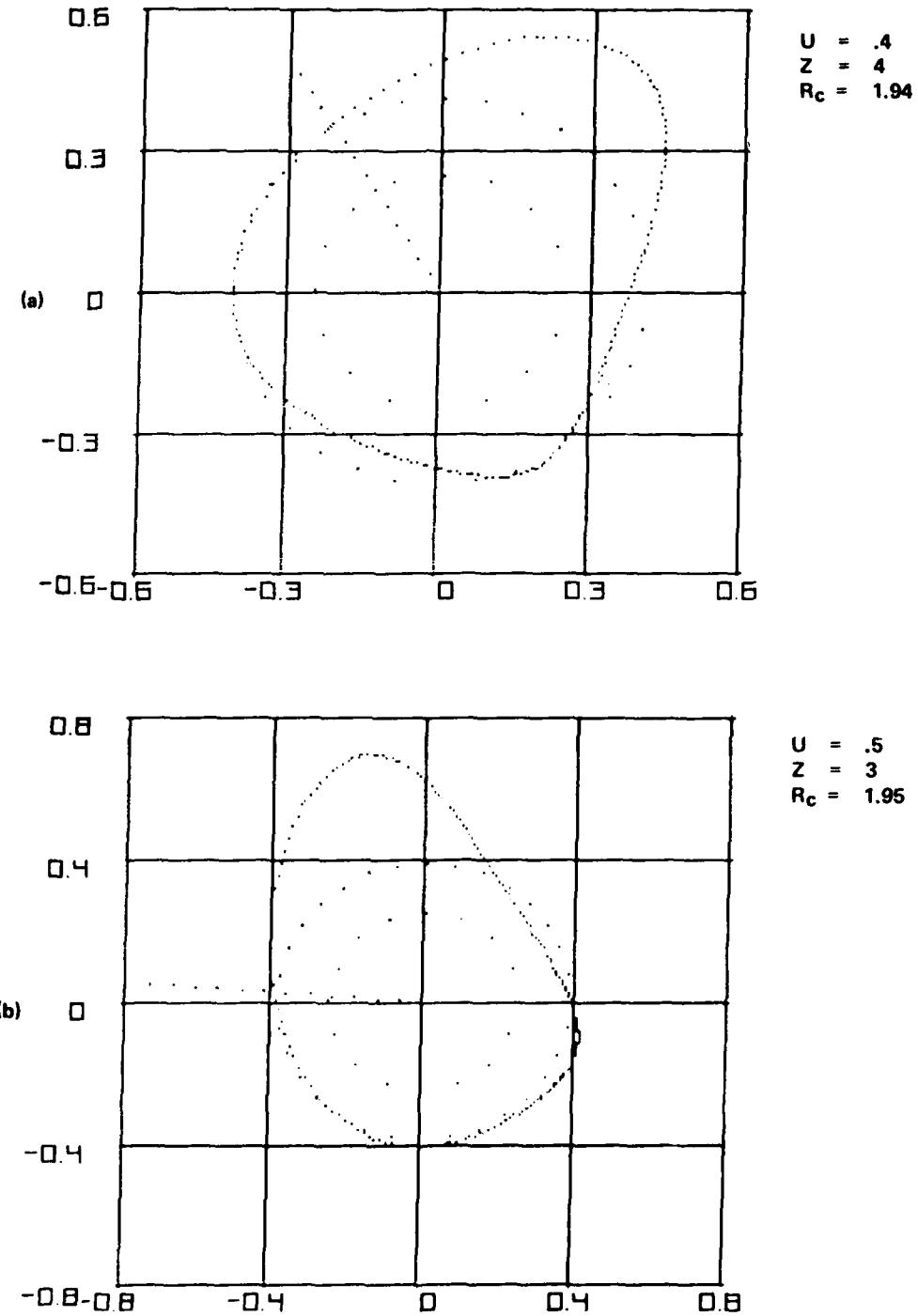

Figure 7.2 Beam cross sections at the position of the output resonator for the last two cases listed in Table 7.
a) U = 0.4, perveance = 0.36 x 10^{-6}
b) U = 0.5, perveance = 0.55 x 10^{-6}

The fact that the RF beam cross section is different from the dc beam cross section merely confirms the previously described RF focusing and defocusing effect.

7.1.1 Optimized Detuning of Cavities

The performance in Table 7.1 was calculated with all cavities tuned to resonance. It turns out that a slight inductive detuning of the last two cavities increases the gain considerably. The reason for the increase is a more favorable phase of the RF deflecting field, causing better correspondence of the relative phases between transverse velocity and displacement. The effect is to improve the cumulative adding of contributions to the gain from the various cavities.

Case 3 in Table 7.1 was investigated with regard to optimum tuning, using a trial procedure. The comparison between the original synchronous tuning and the optimum tuning is shown in Table 7.2. The cavity detuning is specified by the relative frequency parameter $\delta = (f - f_o)/f_o$.

The detuning has a marked effect on the three-cavity system, increasing the overall gain from 51 dB to 68 dB. The device should therefore incorporate means for tuning adjustments in order to optimize the gain.

TABLE 7.2

GAIN COMPARISON OF THE SYNCHRONOUSLY TUNED SYSTEM AND THE OPTIMALLY TUNED SET OF DEFLECTION CAVITIES.
Q_o = 5000 FOR ALL CAVITIES.
TUNING PARAMETER $\delta = (f - f_o)/f_o$.

Tuning	Deflection Angle U (radians)	Beam Perveance ($\mu A/V^{3/2}$)	Power Gain (dB)		
			Cavity 1	Cavity 2	Cavity 3
Synchronous (δ)	0.4	0.36	10.6 (0)	30.6 (0)	50.7 (0)
Optimum (δ)	0.4	0.36	10.6 (0)	38.8 (-0.0004)	67.6 (-0.0002)

The beam cross sections for the two cases in Table 7.2 are presented in Figure 7.3. As expected, the detuning results in a different phase of the beam location. This is reflected in the figures as a rotation of one pattern with respect to the other. In addition, the detuned case is characterized by different beam symmetry with respect to the tube axis.

The significant increase in gain by proper tuning suggests that a two-cavity system might be adequate as far as gain is concerned. The interesting possibility of broadbanding by stagger tuning has not been investigated, but could easily be undertaken by proper modifications in the existing computer program.

7.1.2 The Effect of Lowering the Q-Values

The previous examples were all run with unloaded Q-values of 5000. In order to obtain an idea of how much the gain is lowered by reducing the Q from 5000 to 1000, i.e., by a factor of five, we went through the same procedure as in Table 7.2, but with $Q_o = 1000$. The results are shown in Table 7.3. The optimum tuning scheme still has more than 45 dB gain for the three-cavity system. In general, it appears that the gain is reduced by about 4 dB in the one-cavity system, by 13 dB in the two-cavity system, and by 20 dB in the three-cavity system.

7.1.3 Very High RF Power

The following results demonstrate the feasibility of operation at quite high power levels, in the example 22 MW. Gain calculations were made with $V_o = 250$ kV, perveance = 0.7×10^{-6}, deflection angle = 0.5 and Q-values of 1000. The combination of beam data satisfied the optimum conditions specified in Equation (5.8). In particular, the value of $\alpha^2 U$ is only a slightly above 0.2, and accordingly we do not expect much difficulty with excessive RF beam distortion. This is confirmed by the

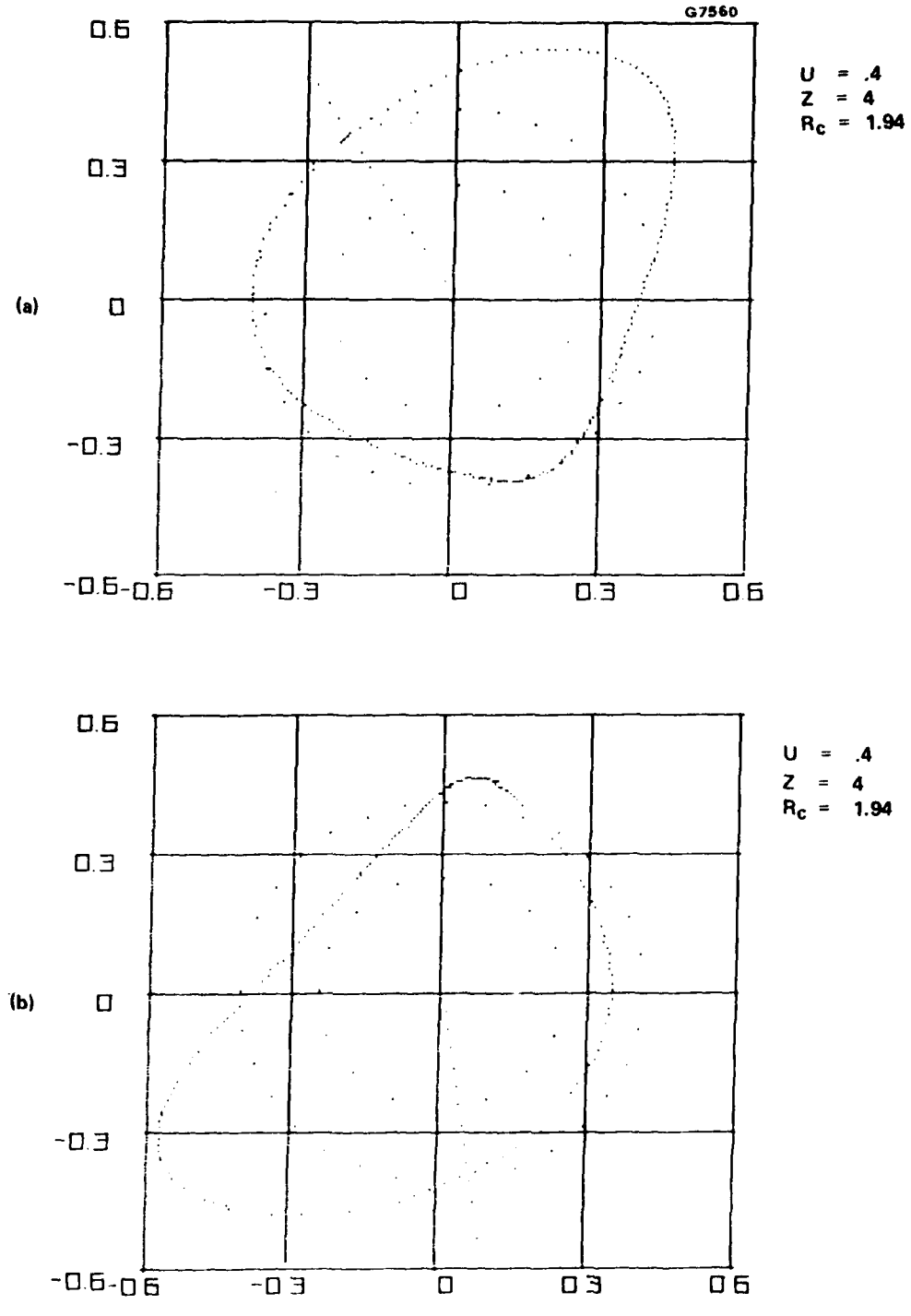

Figure 7.3 Beam cross sections at the location of the output resonator for the two cases listed in Table 7.2.
a) Synchronous tuning
b) Optimum tuning.

TABLE 7-3

GAIN COMPARISON OF THE SYNCHRONOUSLY TUNED SYSTEM AND THE OPTIMALLY TUNED SET OF DEFLECTION CAVITIES.
Q_o = 1000 FOR ALL CAVITIES.

Tuning	Deflection Angle U (radians)	Beam Perveance ($\mu A/V^{3/2}$)	Power Gain (dB)		
			Cavity 1	Cavity 2	Cavity 3
Synchronous (δ)	0.4	0.36	6.3 (0)	17.8 (0)	30.4 (0)
Optimum (δ)	0.4	0.36	6.3 (0)	25.9 (-0.001)	47.0 (-0.0007)

results listed in Table 7.4, and, in particular, by Figure 7.4 showing the beam cross section at the location of the output resonator. Only the usual RF focusing effects are present. The gain of the three-cavity, low Q system is as high as 62 dB.

TABLE 7.4

GAIN OF AN OPTIMALLY TUNED SYSTEM OPERATING WITH A BEAM POWER OF 22 MW AT 250 kV

Tuning	Deflection Angle U (radians)	Beam Perveance ($\mu A/V^{3/2}$)	Power Gain (dB)		
			Cavity 1	Cavity 2	Cavity 3
Optimum (δ)	0.5	0.70	8.4 (0)	34.9 (-0.0015)	62.5 (-0.001)

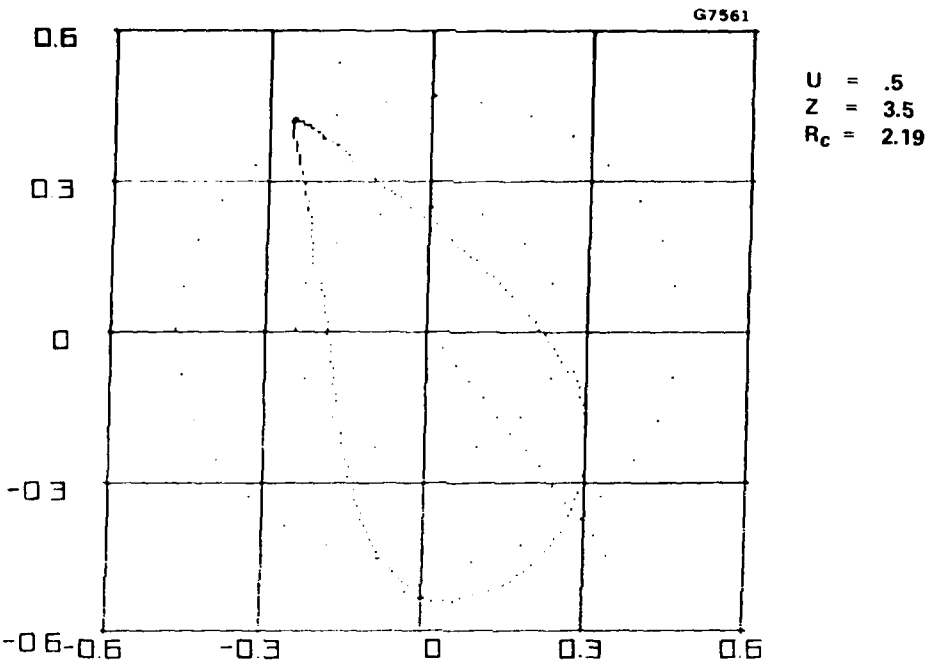

Figure 7.4 Beam cross section at the location of the output cavity for the 22 MW deflection system specified in Table 7.4.

The example certainly confirms that operation at high power levels with fairly high perveance is possible, provided the beam voltage is sufficiently high.

7.1.4 Excessive RF distortion and Overtaking Phenomena

RF distortion and overtaking effects were discussed earlier in Section 5.2, but we have not seen overtaking in the presented graphs of beam cross sections. The explanation for this is that the results so far all refer to the optimum combination of deflection angle, perveance, and beam cross section, specified by (5.8) or the universal design curves in Figure 5.3. What is even more important, we have used the smallest possible radius of the output resonator, which is $R_c = 2$. A larger resonator radius calls for a longer drift space, and an aggravation of the distortion due to longer drift.

As an example we have taken Case 2 in Table 7.1, increased the normalized drift distance from 6 to 13, and reduced the deflection angle from 0.3 to 0.15, thereby maintaining the same value of $R_c \approx 2$. The minimum beam radius is also changed from 0.25 to 0.4.

The plot in Figure 7.5 shows the distorted cross sections of different parts of the beam, corresponding to $R_0 = 0.4$, $R_1 = 0.3$, $R_2 = 0.2$ and $R_3 = 0.1$. The curves exhibit the figure eight shape, discussed earlier in connection with Figure 4.2, which is characteristic of azimuthal overtaking. The figure also reveals a small amount of radial overtaking for some of the electrons located near the beam edge. Only the central parts of the beam are free from overtaking phenomena, exhibiting the near ellipsoidal shape which is typical of an RF focused thin beam.

A large number of computer runs with various combinations of parameters indicate that the safest way of avoiding excessive beam distortion is to

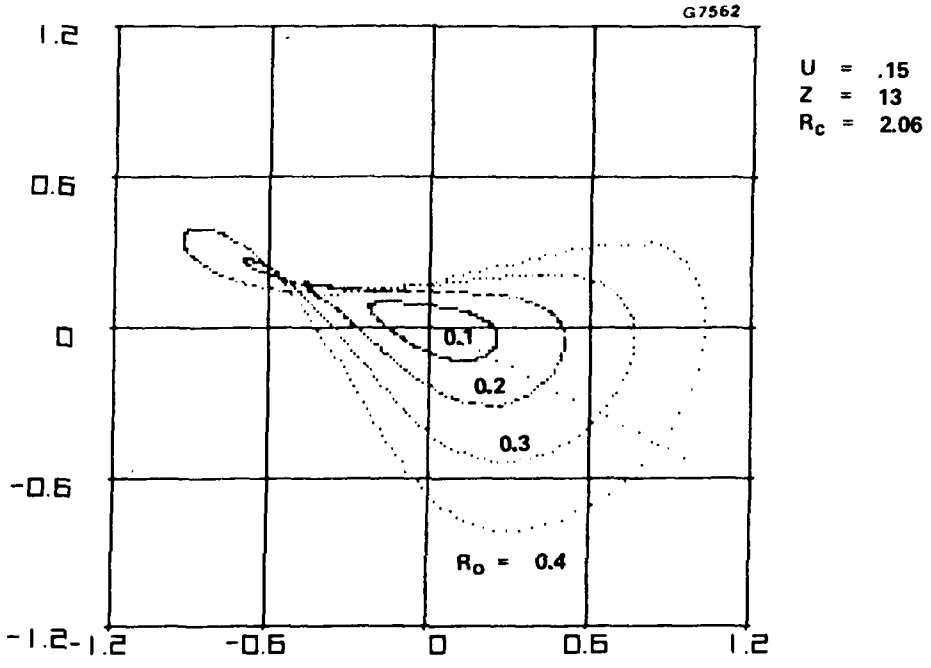

Figure 7.5 Illustration of excessive beam distortion and RF overtaking phenomena. Except for R_0 = 0.4, U = 0.15, and twice the drift distance, the plot corresponds to Case 2 in Table 7.1.

maintain optimum combination of parameters specified by the design curves in Figure 5.3, and, in addition, use the smallest possible radius in the output resonator, which is $R_c \approx 2$.

The last point implies that the output traveling-wave resonator should have the same group and phase velocity, because only in this case can we have $R_c \approx 2$. This condition is satisfied by an oversize waveguide or by a TEM transmission line. Further discussion of the output resonator is beyond the scope of the present investigation.

8.0 CONCLUSIONS

The present study of the deflection system in deflection modulated microwave generators has demonstrated that these devices can be designed with some very attractive features.

It has been shown that high gains can be obtained by using multicavity deflection systems. Only the first cavity is driven by an RF input signal, while in subsequent deflection cavities the RF fields are excited by the modulated beam. Typical power gains are 10-15 dB for a single deflection cavity, 30 dB for a two-cavity system, and 50 dB for a three-cavity system. The high gain eliminates the need for dc deflection magnets. This considerably simplifies both the analytical design and the physical construction of the device.

A key element in the present design approach is the use of electric deflection cavities instead of magnetic deflection cavities. It was estimated that the effective interaction strength is typically ten times larger for electric deflection compared to magnetic deflection. Furthermore, due to a novel design concept, only a single input signal is required to provide a circular deflection of the electron beam, whereas ordinarily two signals 90 degrees out of phase are needed.

Suitable power levels for gyrocon operation range from a hundred kilowatts to tens of megawatts. In general, the deflection system does not appear to be the limiting factor in gyrocon design. Although the operating bandwidth is expected to be narrow, the possibility of using stagger tuning or coupled deflection cavities for wider frequency response of the deflection system exists. Most major characteristics of gyrocons, such as efficiency, bandwidth, and high frequency limitation, are chiefly determined by the output cavity. A study of the output cavity is therefore essential to resolve many questions concerning the potential performance and capability of deflection modulated microwave amplifiers.

AD-A090 027 HUGHES AIRCRAFT CO TORRANCE CALIF F/G 9/5
HIGH EFFICIENCY DEFLECTION MODULATED MICROWAVE GENERATOR STUDY.(U)
JUL 80 T WESSEL-BERG, I TAMMARU F30602-79-C-0089
UNCLASSIFIED W-08322 RADC-TR-80-211 NL

2 OF 2
AD A 090027

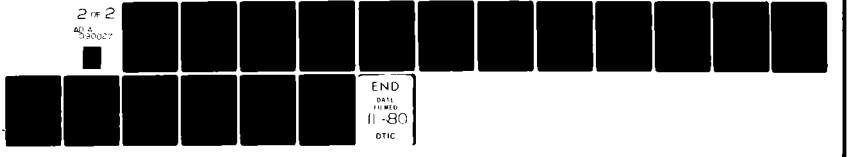

END
DATE FILMED
11-80
DTIC

APPENDIX A. A COMPARISON OF TE AND TM DEFLECTING CAVITIES

We shall make a comparison between the relative merits of the open TE-type deflection cavity used in the present investigation and the shorted type TM_{110} used in the original type gyrocons.[1-3]

As a figure of merit, the characteristic impedance R_{sh}/Q is the appropriate parameter:

$$\frac{R_{sh}}{Q} = \frac{1}{2\omega}\frac{V^2}{W} \quad , \tag{A.1}$$

where W is the stored energy in the resonator and V is the RF voltage defined proportional to the integrated transverse force experienced by the beam in passing through the cavity. Let us evaluate the ratio of V^2/W for the two cavity types.

A.1 THE OPEN TE CAVITY

The basic configuration is two parallel deflection plates as shown in Figure 3.2 in the main text. The major part of the electric energy is stored between the plates whereas the magnetic energy is stored in the part of the cavity which is outside the plates.

Making allowance for transverse beam displacement let us take the plate spacing d to be a factor γ larger than the beam diameter. If E is the transverse electric field, the stored energy per unit length is given by

$$W_e = \frac{1}{2}\epsilon_0 E^2 d^2 \quad , \tag{A.2}$$

where we have assumed that the plate width is equal to the plate spacing d. The following ratio is representative of the characteristic impedance:

$$\frac{E^2}{W_e} = \frac{2}{\varepsilon_o d^2} = \frac{0.5\ \beta_e^2}{\varepsilon_0 \gamma^2 R_0^2} \quad , \tag{A.3}$$

where R_0 is the normalized beam radius, and the plate spacing-to-beam diameter ratio γ is larger than one.

A.2 THE TM_{110} CAVITY

The stored energy is evaluated from the longitudinal E-field:

$$E_z(r, \theta) = A\ J_1(k_c r)\ \sin n\theta \tag{A.4}$$

At the beam axis the transverse force $v_0 B$ is given by

$$v_0 B = \frac{v_0}{c} \frac{A}{2} \tag{A.5}$$

The stored energy per unit length is:

$$W_e = \frac{1}{2} \varepsilon_0 \int_0^a \int_0^{2\pi} E_z^2\ r dr d\phi \tag{A.6}$$

Evaluating the integral with the proper boundary condition of $E_z = 0$ at the external wall we find:

$$\frac{(v_0 B)^2}{W_e} = \left(\frac{v_0}{c}\right)^2 \frac{6.25}{\varepsilon_0 a^2} \quad , \tag{A.7}$$

where a is the radius of the TM_{110} cavity. The radius must satisfy the resonance condition

$$\frac{\omega}{c} a = 3.83 \tag{A.8}$$

Using this expression we can rewrite (A.7) as follows:

$$\frac{(v_0 B)^2}{W_e} = 0.42 \left(\frac{v_0}{c}\right)^4 \frac{\beta_e^2}{\varepsilon_0} \tag{A.9}$$

Let us determine the ratio of the characteristic impedances by dividing (A.9) and (A.3). The result is

$$\frac{(R_{sh}/Q)_{TM}}{(R_{sh}/Q)_{TE}} = 0.84 \left(\frac{v_0}{c}\right)^4 \gamma^2 R_0^2 \tag{A.10}$$

As noted in the main text, R_0 is typically 0.25. We expect γ to be between 2 and 4. So let us put $\gamma = 3$, and evaluate (A.10) with these numbers. We obtain

$$\frac{(R_{sh}/Q)_{TM}}{(R_{sh}/Q)_{TE}} \approx 0.5 \left(\frac{v_0}{c}\right)^4 \tag{A.11}$$

For a 90 kV beam the ratio $v_0/c = 0.53$, which inserted into (A.11) yields

$$\frac{(R_{sh}/Q)_{TM}}{(R_{sh}/Q)_{TE}} \approx 0.038 \tag{A.12}$$

The example shows that the TM cavity at 90 kV is expected to be roughly 25 times less efficient than the open TE cavity.

The situation is less serious for the TM cavity at extremely high voltages. For a 250 kV beam the ratio is given by

$$\frac{(R_{sh}/Q)_{TM}}{(R_{sh}/Q)_{TE}} \approx 0.15 \qquad (A.13)$$

Admittedly, the present comparison is based on several approximations concerning the actual fields and their distribution in the open TE cavity. Nevertheless, the results are considered accurate enough for a first estimate.

Apparently, the effectiveness of the TM cavity suffers in two ways: First, the deflecting force is proportional to v_0B, i.e., to the dc velocity v_0. Second, the magnetic field of the cavity cannot be confined to essentially the space occupied by the beam, as is the case for the TE-cavity. The overall effect is a reduction of characteristic impedance by the factor v_0/c to <u>fourth</u> power.

One might argue that the smaller characteristic impedance in the TM cavity can be offset by a correspondingly higher Q-value, but this argument has only limited value. The loaded Q-value is determined by the <u>combined</u> circuit loss and beam loading loss, and it makes no sense to increase Q beyond a fairly low value (approximately 5,000 in most of the computer runs with the parallel plate cavity).

Moreover, if one is designing an amplifier with a certain bandwidth requirement, as may or may not be the case, the R_{sh}/Q is the relevant parameter determining the gain-bandwidth product.

In conclusion, the open TE parallel plate cavity appears to be considerably more efficient than the TM_{110} cavity type used in the original gyrocons.

APPENDIX B
PERTURBATION FORMULAS

If a cavity resonating at frequency f_o is perturbed by a foreign object characterized by permittivity ε and permeability μ, the cavity resonance, for small perturbations, shifts by an amount Δf given by[9]

$$\frac{\Delta f}{f_o} = -\frac{1}{4W}\int_V \left[(\varepsilon - \varepsilon_0)\,\vec{E}\cdot\vec{E}_0^{\,*} + (\mu - \mu_0)\,\vec{H}\cdot\vec{H}_0^{\,*}\right] d\tau \qquad (B.1)$$

Here $\vec{E}_0$, $\vec{H}_0$ and $\vec{E}$, $\vec{H}$ are the fields before and after the perturbation, and W is the total energy in the cavity. The volume integral is nonzero only over the perturbing object.

B.1 PERTURBATION BY DIELECTRIC ROD

With a dielectric rod parallel to the electric field, we have $\vec{E} \approx \vec{E}_0$. This gives

$$\frac{\Delta f}{f_0} = -\frac{(\varepsilon - \varepsilon_0)\,\pi r_d^2 \ell_d \langle E^2\rangle}{4W}\,, \qquad (B.1)$$

where the E-field has been assumed constant over the rod cross section (area πr_d^2), and $\langle E^2\rangle$ is the average value of E^2 over the rod length ℓ_d. Thus

$$\frac{\varepsilon_0\langle E^2\rangle}{W} = -\frac{4}{\pi\,(\varepsilon/\varepsilon_0 - 1)\,r_d^2\ell_d}\left(\frac{\Delta f}{f_0}\right) \qquad (B.2)$$

B.2 PERTURBATION BY SMALL SPHERICAL BEAD

If a small spherical bead is inserted into a region of approximately uniform electric and magnetic fields $\vec{E}_0$ and $\vec{H}_0$, the perturbed fields in the bead are

$$\vec{E} = \frac{3\epsilon_0}{\epsilon + 2\epsilon_0} \vec{E}_0 \tag{B.3}$$

$$\vec{H} = \frac{3\mu_0}{\mu + 2\mu_0} \vec{H}_0 \tag{B.4}$$

A dielectric bead, with $\mu = \mu_0$, does not affect the magnetic field. The relation (B.1) then gives

$$\frac{\epsilon_0 E_0^2}{W} = -\frac{1}{\pi r_d^3}\left(\frac{\kappa + 2}{\kappa - 1}\right)\frac{\Delta f_d}{f_0} \quad , \tag{B.5}$$

where $\kappa = \epsilon/\epsilon_0$ = relative dielectric constant, r_d is the radius of the sphere, and E_0 is the unperturbed field at the center of the sphere.

For a perfectly conducting metal bead $\mu = 0$ and $\epsilon \to \infty$. Over the volume of the sphere the expression under the integral sign in (B.1) becomes

$$(\epsilon - \epsilon_0)\, \vec{E} \cdot \vec{E}_0^{\,*} + (\mu - \mu_0)\, \vec{H} \cdot \vec{H}_0^{\,*} = 3\epsilon_0 E_0^2 - \frac{3}{2}\mu_0 H_0^2 \tag{B.6}$$

The result is

$$\frac{\epsilon_0 E_0^2}{W} - \frac{1}{2}\frac{\mu_0 H_0^2}{W} = \frac{1}{\pi r_m^3}\frac{\Delta f_m}{f_0} \quad , \tag{B.7}$$

where r_m is the radius of the metal sphere. Solving for the magnetic field, using (B.5), we find

$$\frac{\mu_0 H_0^2}{W} = \frac{2}{\pi r_m^3} \frac{\Delta f_m}{f_0} - \frac{2}{\pi r_d^3}\left(\frac{\kappa + 2}{\kappa - 1}\right)\frac{\Delta f_d}{f_0} \qquad \text{(B.8)}$$

REFERENCES

1. G. I. Budker, et al., "High-frequency system of the VEPP-4 electron-position storage ring, based on the gyrocon - a powerful ultrashort wave generator with an unbunched relativistic beam." Paper presented at a conference August 1977 (Translation for Stanford Linear Acceleration Center, Stanford, California).

2. P. J. Tallerico, "The gyrocon: A deflection-modulated high power microwave amplifier," Los Alamos Scientific Laboratory, Los Alamos, NM, Technical Report UC-28, October 1977.

3. P. J. Tallerico and J. E. Rankin, "The gyrocon: A high-efficiency high-power microwave amplifier," IEEE Trans Ed, vol ED-26, pp. 1559-1566, Oct. 1979.

4. T. Wessel-Berg, "A new concept for generation of multi-megawatt power approaching hundred percent efficiency," University of Trondheim, Norway, Paper presented at the International Electron Device Meeting, Washington, D.C., December 1977.

5. W.K.H. Panofsky and W. A. Wenzel, "Some considerations concerning the transverse deflection of charged particles in radio-frequency fields," Rev. Sci. Instr. 27, 967 (1956).

6. K. H. Kreuchen, B. A. Auld, and N. E. Dixon, "A study of the broadband frequency response of the multi-cavity klystron amplifier," J. Electronics 2, 529-67 (1957).

7. S. Ramo, J. R. Whinnery, and T. van Duzer, "Fields and Wave in Communication Electronics," John Wiley & Sons, 1965, Chapter 10.

8. G. B. Collins (editor), "Microwave Magnetrons," MIT Rad. Lab. Series, Vol. 6, McGraw Hill, 1948.

9. W. R. Smythe, "Static and Dynamic Electricity," 3rd Edition, McGraw Hill, 1968, Chapter 13.

LIST OF SYMBOLS

a	radius of cylindrical cavity
$\vec{a}_z$	unit vector in z direction
$\vec{B}$	magnetic induction vector
$B_z(X, Y, Z)$	z component of magnetic induction
$\hat{B}^{(1)}_{zx}(Z)$	first-order gradient in the x direction of $B_z(X, Y, Z)$
$\hat{B}^{(1)}_{zy}(Z)$	first-order gradient in the y direction of $B_z(X, Y, Z)$
$\hat{B}^{(0)}_{+}(Z)$	zero-order value of the positive polarized component of transverse magnetic field
c	speed of light; deflection plate width
C_1	constant, p. 32
d	plate separation
e	charge of electron
$\vec{E}$	electric field vector
E_o	electric field at center of deflection cavity
$E_z(X, Y, Z)$	z component of electric field
$\hat{E}^{(1)}_{zx}(Z)$	first-order gradient in the x direction of $E_z(X, Y, Z)$

$E_{zy}^{(1)}(Z)$	first-order gradient in the y direction of $E_z(X, Y, \_)$
$E_+(X, Y, Z)$	positive polarized component of transverse electric field
$E_-(X, Y, Z)$	negative polarized component of transverse electric field
$\hat{E}_+^{(0)}(Z)$	zero-order value of $E_+(X, Y, Z)$
f	frequency
f_o	resonant frequency
$f_{(mnp)}$	resonance frequency of TE_{mnp} mode
g_c	normalized circuit conductance
g_{es}	normalized electronic conductance of sth cavity
G_c	circuit conductance
G_{e+}	electronic conductance of the positive polarized component
I_o	dc beam current
J_m	Bessel function of order m
ℓ	length of interaction region
ℓ'	distance between center planes of composite cavity
ℓ_o	plate length
L_o	normalized plate length

L_N	normalized length of the Nth cavity
L_{Np}	normalized spacing between centers of the pth and Nth cavities
m	relativistic electron mass
m_o	rest mass of electron
M_+	coupling coefficient of the positive polarized component
N	the last cavity
p	the pth cavity; number of half sine waves
P_o	dc beam power
P_i	input RF power
P	power loss in a cavity
Q	Q-value of a cavity
r	dc beam radius; cavity radius
r_o	minimum dc beam radius
r_0, r_1, r_2	cavity spacer iris radius
r_b	beam radius
r_c	radius of output resonator
r_d	radius of dielectric rod or bead

r_m	radius of spherical metal bead
R	normalized radius of the dc beam at the output cavity
R_o	normalized radius of the dc beam at the minimum
R_c	normalized radius of output cavity
$\vec{R}_D$	normalized position vector
R_{sh}	cavity shunt impedance
$\vec{s}$	displacement vector
$\vec{S}$	normalized displacement
s_0, s_1, s_2	spacer thickness
$\hat{S}^{(0)}_{+N}$	zero-order normalized positive polarized displacement at the exit of last deflection cavity
S_N	absolute value of $S^{(0)}_{+N}$
t	time; plate thickness
T	normalized time
$\vec{u}$	RF velocity vector
U	deflection angle at exit of last deflection cavity
$\vec{U}(\vec{r}, t)$	normalized RF velocity
U_+	positive polarized component of $\vec{U}(\vec{r}, t)$

U_-	negative polarized component of $\vec{U}(\vec{r}, t)$
$\hat{U}_{+N}^{(0)}$	zero-order normalized positive polarized component at the exit of last deflection cavity
U_N	absolute value of $U_{+N}^{(0)}$
$\vec{v}(\vec{r}, t)$	total electron velocity
v_o	dc beam velocity
V_o	dc beam voltage
v_{ph}	phase velocity of output resonator
V_+	positive polarized RF voltage in a cavity
V_{+1}	positive polarized RF voltage of the input cavity
w	plate support thickness
W	total stored energy in cavity
X	normalized x coordinate
X_D	x component of $\vec{R}_D$
Y	normalized y coordinate
Y_D	y component of $\vec{R}_D$
Y_c	circuit admittance
y_{cs}	normalized circuit admittance of sth cavity

Y_{np}	transfer admittance between cavity p and n, where n > p
Z	normalized longitudinal coordinate in drift space
Z_D	z component of $\vec{R}_D$
α	relativistic factor, $\sqrt{1 - (v_o/c)^2}$
β_e	electronic propagation factor
γ	ratio of plate spacing to beam diameter
δ	frequency tuning parameter
Δf	frequency shift with perturbation
$\delta\hat{U}_{+n}^{(0)}$	deflection sensitivity
$\delta\hat{S}_{+n}^{(0)}$	displacement sensitivity
ε	permittivity of dielectric material
ε_o	permittivity of vacuum
η_p	voltage gain in pth cavity
$\eta_{s,r}$	feed-forward gain between rth and sth cavities, where s > r
θ	argument of $U_{+N}^{(0)}$
κ	relative dielectric constant
μ	permeability

μ_o	permeability of vacuum
ξ	plate length parameter
ϕ	argument of $\hat{S}_{+N}^{(0)}$
ω	angular frequency

MISSION
of
Rome Air Development Center

RADC plans and executes research, development, test and selected acquisition programs in support of Command, Control Communications and Intelligence (C^3I) activities. Technical and engineering support within areas of technical competence is provided to ESD Program Offices (POs) and other ESD elements. The principal technical mission areas are communications, electromagnetic guidance and control, surveillance of ground and aerospace objects, intelligence data collection and handling, information system technology, ionospheric propagation, solid state sciences, microwave physics and electronic reliability, maintainability and compatibility.